J. Fluid Mech. (1968), *vol.* 32, *part* 3, *pp.* 489–528
Printed in Great Britain

On standing internal gravity waves of finite amplitude

By S. A. THORPE
National Institute of Oceanography, Wormley, Godalming, Surrey

(Received 30 June 1967)

Two-dimensional internal gravity waves in a rectangular container are examined theoretically and experimentally in (*a*) fluids which contain a single density discontinuity and (*b*) fluids in which the density gradient is everywhere continuous. The fractional density difference between the top and bottom of the fluid is small.

Good agreement is found between the observed and calculated wave profiles in case (*a*). Unlike surface standing waves, which tend to sharpen at their crests as the wave amplitude increases, and which eventually break at the crests when fluid accelerations become equal to that of gravity, internal wave crests are found to be flat and exhibit no instability. In the case (*a*) breaking is found to occur at the nodes of the interfacial wave, where the current shear, generated by the wave itself, is greatest. For sufficiently large wave amplitudes, a disturbance with the form of a vortex but with direction of rotation reversing twice every cycle, grows at the wave node and causes mixing. This instability is found to be followed by the generation of cross-waves, of which two different forms are observed.

Several modes of oscillation can be generated and are observed in a fluid with constant density gradient. The wave frequencies and shape are well predicted by theory. The experiments failed to establish any limitation of the possible wave amplitudes.

1. Introduction

This investigation is concerned with two-dimensional standing internal gravity waves in an incompressible and inviscid, stably stratified fluid confined within a rectangular container with vertical walls. Standing internal waves are commonly found in lakes (internal seiches) and have been studied by a number of people, notably Wedderburn & Williams (1911) and more recently Mortimer (1952). Oscillations interpreted as standing waves have been recorded in the Norwegian fjords (Pettersson 1909; Wedderburn 1909). The work reported here was primarily experimental and was done in the hope of gaining insight into the dynamics of breaking internal waves in controlled laboratory conditions.

Before discussing standing waves in stratified fluids, we shall outline what is known theoretically and experimentally about standing surface gravity waves, so that comparisons may be borne in mind between these and the present findings. The theoretical study of standing waves really dates back to the paper by Stokes in 1847 in which the first-order linear solutions for both progressive

surface and interfacial waves (those at an interface between two fluids each of constant density) were found. By superimposing two equal linear wave trains travelling in opposite directions, a first-order solution for standing waves may be found. It was not until over a century later that the work of Stokes as applied to standing surface waves was developed further by Penney & Price (1952) to include waves of finite amplitude.† They extended the solution to fifth order for surface waves in deep water and produced a theory which predicted that the crest of the highest stable standing wave would enclose a right angle. The latter theory was discredited by Taylor (1953) although an experiment confirmed that in fact the prediction was good. Taylor generated standing waves by oscillating two flaps at the ends of a tank of water, and by gradually increasing the amplitude of the flap oscillation and adjusting the frequencies was able to produce waves enclosing an angle at their crests which was very close to 90°, after which instability occurred. This instability was examined, and it was found that, following a little wave breaking by splashing after the critical amplitude had been exceeded, cross-waves of half the flap frequency were set up in the water, and the two-dimensional motion could no longer be maintained. Tadjbakhsh & Keller (1960) further extended the theory to waves in shallow water by an expression to third order. The equation of the wave profile to second order is

$$\eta = a \sin \sigma t \cos kx + \tfrac{1}{8} a^2 k [T - T^{-1} + T^{-3}(T^2 - 3) \cos 2\sigma t] \cos 2kx \qquad (1.1)$$

and the dispersion relation (to third order)

$$\sigma^2 = gkT\left(1 - \frac{a^2k^2}{32T^4}[2T^6 + 3T^4 + 12T^2 - 9]\right), \qquad (1.2)$$

where k is the wave-number, σ the frequency, a is a constant proportional to the wave amplitude, h is the fluid depth and T is written for $\tanh kh$.

It will be seen that the effect of the second-order terms is to distort the sinusoidal wave-form so that the profile of these surface waves is always such that the crests are narrower and sharper than the troughs, no matter what the fluid depth, and this effect is indeed observed. Moreover, the dependence of frequency on the wave slope, ak in the dispersion relation changes sign. For values of depth to wavelength ratio, h/λ, greater than 0·17, the frequency decreases as the wave amplitude increases, whilst for $h/\lambda < 0{\cdot}17$ the frequency increases. This remarkable prediction led Fultz (1962) to test the conclusions by experiment. Fultz found that the change in dependence does exist but at a slightly lower value of h/λ ($= 0{\cdot}14$), a result recently confirmed by Marcou (1965) in an independent experiment.

The cross modes observed by Taylor were investigated by Lin & Howard (1960) both experimentally and theoretically. Their main conclusions were (*a*) that the cross-mode is the result of an interaction between the wave-making flap and the finite amplitude wave, and that a critical flap amplitude must be exceeded before the cross-mode develops, (*b*) that the cross-mode has half the frequency of the wave flap; (*c*) certain critical frequencies are necessary to excite

† At about the same time a third order theory was published by Sekerzh-Zenkovich (1951).

the cross-mode; (*d*) there are certain tank width to length ratios which are most favourable for cross-wave development; (*e*) there is a phase angle of 90° between the wave flap and the cross-wave motion.

An experimental study of the mean secondary currents in the plane of the wave motion was made by Ayrton (1908, 1926), but there is no reference to currents at right angles to this plane in the surface of the water.

The ease with which Taylor caused breaking of the surface in the wave motion during his experiments suggested that an experimental study of interfacial standing waves and waves in other density profiles might lead to information about how internal waves break and, more generally, about the factors affecting the stability of fluid systems which are stably stratified.

Little theoretical or experimental work on standing internal waves has been done. Two theoretical papers were published at about the same time in 1961, both on standing interfacial waves in deep fluids making an expansion similar to that of Penney & Price, one by Hunt and the other by Sekerzh-Zenkovich. That of Hunt extends the theory to fourth order. It was found that, to third order, the equation of the interface is

$$\zeta(x,t) = a\left[\sin\sigma t + \frac{a^2k^2(\rho_2^2-\rho_1\rho_2+\rho_1^2)}{16(\rho_1+\rho_2)^2}\sin 3\sigma t\right]\cos kx + \frac{a^2k}{4}\frac{\rho_2-\rho_1}{\rho_1+\rho_2}(1-\cos 2\sigma t)\cos 2kx + \frac{a^3k^2}{32}\frac{(3\rho_2^2-10\rho_1\rho_2+3\rho_1^2)}{(\rho_1+\rho_2)^2} \times (3\sin\sigma t-\sin 3\sigma t)\cos 3kx, \quad (1.3)$$

and the dispersion relation is

$$\sigma^2 = \frac{gk(\rho_2-\rho_1)}{\rho_1+\rho_2}\left(1-\frac{a^2k^2}{4}\frac{\rho_1^2+\rho_2^2}{(\rho_1+\rho_2)^2}\right), \quad (1.4)$$

where σ is the frequency, k the wave-number, and ρ_1, ρ_2, are the densities of the upper and lower fluids respectively.

Experiments on standing waves in a two fluid system were carried out by Schmidt (1908). His apparatus was a rectangular tank which, when filled, was gently rocked and then held stationary whilst the period of the resulting interfacial wave was measured. The periods found were compared with those predicted theoretically from the linear Stokes theory, and it was found that the predicted periods were 6 % smaller than the observed. Wedderburn & Williams (1911) also experimented with two and three layer models in tanks of various shapes following observations of temperature seiches in the Madüsee.

Schooley & Stewart (1963) found that standing internal waves were generated in their apparatus during an investigation of the flow caused by a self-propelled body in a stratified fluid, but no study of finite amplitude standing internal waves has yet been reported.

The remainder of this paper is divided into two parts. In the first (§2) interfacial waves are examined both theoretically (Hunt's analysis is extended to include finite fluid depths) and experimentally; in the second (§3) waves in a continuously stratified fluid are examined theoretically, and experiments are described which were made in a fluid of constant density gradient.

2. Interfacial waves

2.1. *Theory*

We have extended Hunt's theory to second order in the wave profile, and in the dispersion relation when the density difference is small, for the cases when the upper surface is free and when it is held fixed by a horizontal plane. The method of analysis follows closely that of Penney & Price (1952) and Hunt (1961) and there is no need to elaborate here. (For further details see Thorpe 1966.) The results are complicated and are quoted in full in appendix 1. We shall be here interested only in the case when the density difference between the two fluids is very small and the internal mode is excited, and then the results simplify to the case when the upper boundary is fixed; the equation of the interface to second order is

$$\zeta = a \sin \sigma t \cos kx + \frac{a^2 k}{8 T_1^2 T_2^2} (T_1 - T_2)(T_1 T_2 - 3 \cos 2\sigma t) \cos 2kx, \qquad (2.1.1)$$

where h_1, h_2 are the upper and lower fluid depths respectively, and $T_i = \tanh kh_i$ $(i = 1, 2)$.

The dispersion relation to third order is

$$\sigma^2 = \frac{gk(\rho_2 - \rho_1) T_1 T_2}{\rho_1 T_2 + \rho_2 T_1} \left[1 + \frac{a^2 k^2}{32 T_1^3 T_2^3} (9T_1^2 + 9T_2^2 - 18 T_1 T_2 - 6T_1^3 T_2 - 6T_2^3 T_1 + 8T_1^2 T_2^2) \right]. \qquad (2.1.2)$$

If either kh_1 or kh_2 are large then these expressions reduce to

$$\zeta = a \sin \sigma t \cos kx + (-1)^i (a^2 k / 8T_i^2)(1 - T_i)(T_i - 3 \cos 2\sigma t) \cos 2kx, \qquad (2.1.3)$$

where kh_i remains small, and

$$\sigma^2 = \frac{gk(\rho_2 - \rho_1) T_i}{\rho_i + \rho_j T_i} \left[1 + \frac{a^2 k^2}{32 T_i^2} (9 - 24 T_i + 17 T_i^2 - 6 T_i^3) \right] \quad (i \neq j). \qquad (2.1.4)$$

These equations reduce to Hunt's when both fluids are deep.

Some observations are now made on the physical implications of the above results.

(i) In deep water when the density difference between the fluids is small, we have

$$\zeta = a \left[\left(\sin \sigma t + \frac{a^2 k^2}{64} \sin 3\sigma t \right) \cos kx - \frac{a^2 k^2}{32} (3 \sin \sigma t - \sin 3\sigma t) \cos 3kx \right]$$

from Hunt's result (1.3).

The wave profile is thus symmetrical up and down; there is no cresting. The effect of finite amplitude is to flatten the profile at the crest and trough. The interface becomes completely flat twice every cycle when $t = n\pi/\sigma$ $(n = 0, 1, 2, \ldots)$.

This means that the energy becomes wholly kinetic at these instants, which are the counterparts of the two instants in each cycle when the motion comes wholly to rest.

(ii) When the upper fluid is deep ($kh_1 \gg 1$) and the density difference small, the wave profile is no longer symmetrical but crested upwards at times of maximum

displacement ($t = (2n+1)\pi/2\sigma$) in (2.1.3) and never becomes completely flat having a displacement

$$\tfrac{1}{4}a^2k(T_2^2-1)\cos 2kx \quad \text{at times} \quad t = n\pi/\sigma.$$

(iii) When the lower fluid is deep and density difference small, the profile is as described in remark (ii) above, but inverted, and therefore crested downwards at times of maximum displacement.

(iv) The dispersion relations (2.1.2), (2.1.4) indicate that when the fluids are both deep, the frequency decreases with increasing wave amplitude, whilst if one fluid is deep the trend of frequency decrease is reversed if $\tanh kh_i < 0{\cdot}54$, or if the depth to wavelength ratio is less than about 0·096. The behaviour of σ for varying values of the depths of fluids h_1, h_2 is indicated in figure 1.

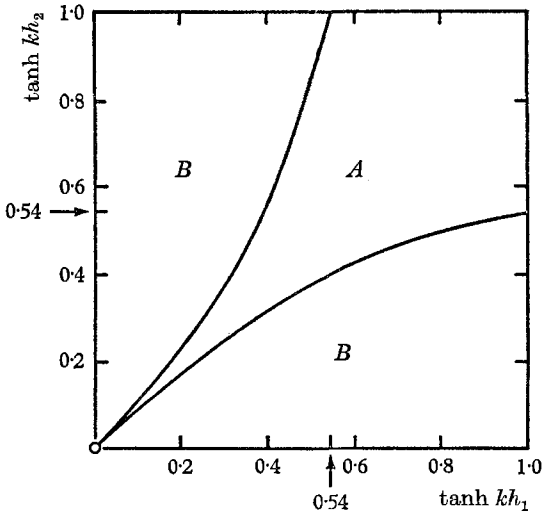

FIGURE 1. The values of tanh kh_1 and tanh kh_2 for which the variation of frequency with wave amplitude changes. In region A the frequency of the standing interfacial waves decreases with increase of wave amplitude; in regions B the frequency increases with increase of wave amplitude.

(v) When the density difference is small, the approximation made in deducing (2.1.1) is valid if

$$\left|\frac{ak(T_1-T_2)(3+T_1T_2)}{8T_1^2T_2^2}\right| \ll 1.$$

If one of the fluids is deep and the other shallow of depth h, this reduces to $3a/8h^2k$, and hence the parameter which must be small is $3a\lambda/16\pi h^2$ in contrast to that of $3a\lambda^2/32\pi^2h^3$ applying to surface waves in fluid of depth h.

2.2. *Experimental results*

It has been found possible to test experimentally some of the conclusions made above. The apparatus and experimental procedure will be described later, but comparison of the observations and predictions may conveniently be made here.

In the experiments, the difference in density between the fluids used was small, being always less than 0·03 g/c.c., while the mean density was not far from 1 g/c.c. Miscible fluids were used; surface tension effects were therefore neglected. The following conclusions were drawn.

(i) In deep water (kh_1, kh_2 both large) the wave profile appeared to be sinusoidal for small wave amplitudes, but became markedly more flattened at the crests

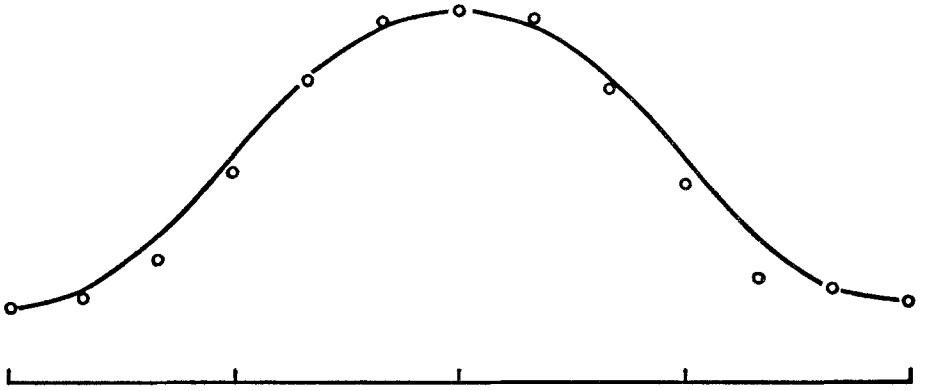

FIGURE 3. Standing wave profile from figure 2*a*. Points measured from 2*a* compared with a sine wave fitted at the crest and trough. The vertical scale is exaggerated.

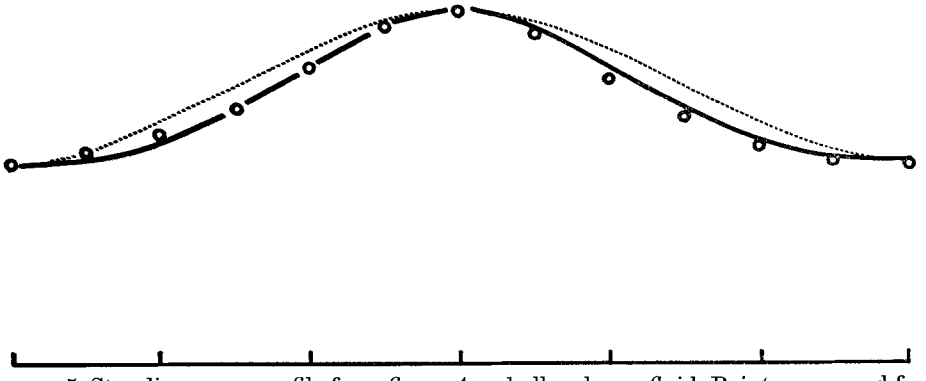

FIGURE 5. Standing wave profile from figure 4*a*, shallow lower fluid. Points measured from 4*a* compared with the second-order theoretical curve (full line) and a sine wave (dashed), both fitted to the experimental points at the wave crest and trough. The vertical scale is exaggerated and the horizontal line marks the level of the bottom of the tank.

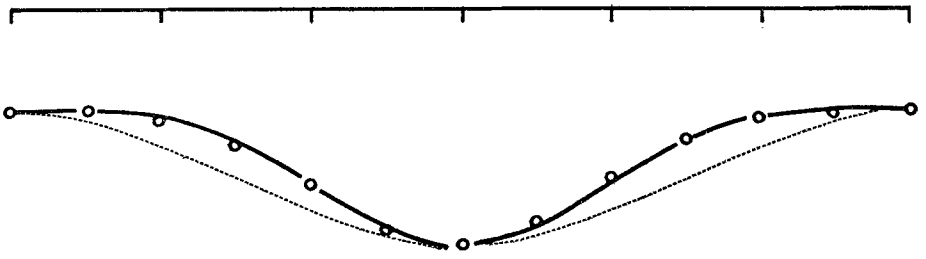

FIGURE 7. Standing wave profile from 6*a*, shallow upper fluid. Points measured from 6*a* compared with the second-order theoretical curve (full line) and a sine wave (dashed), both fitted to the experimental points at crest and trough. The vertical scale is exaggerated and the horizontal line marks the level of the bottom of the tank.

and troughs as the amplitude was increased. Figures 2*a*, *b*, plate 1, show the appearance of the wave in free oscillation and figure 3 shows a comparison of theoretical and observed profiles. The points on the graph taken from the observed profiles were measured from a curve drawn from the projected and enlarged image of the photographs. The profile appeared to be flat once every half cycle, as predicted.

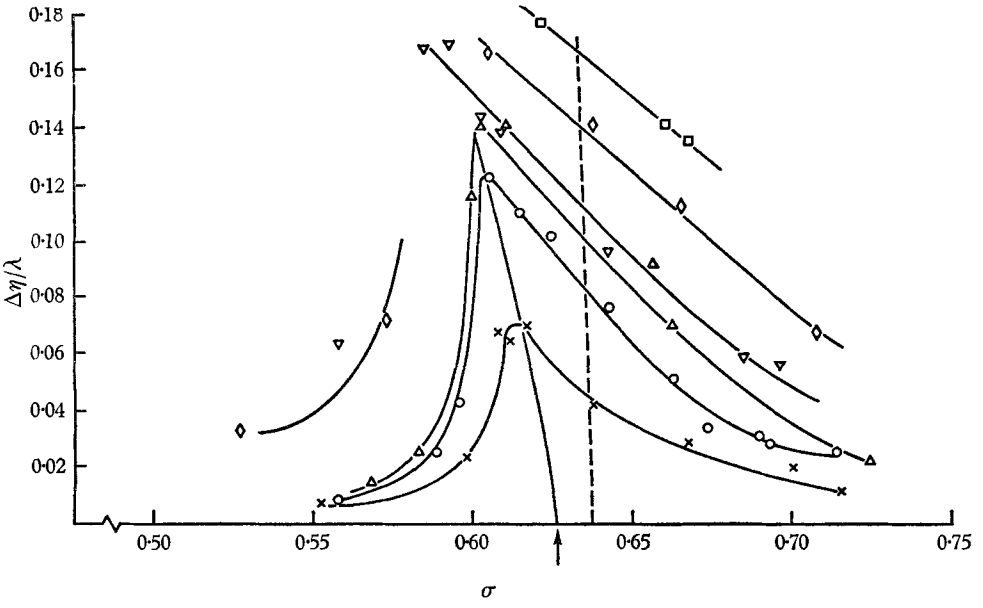

FIGURE 8. Response curves for interfacial waves in deep fluids with a density difference $4{\cdot}7 \times 10^{-3}$g/c.c. The plunger frequency σ is measured in radians per second, $\Delta\eta$ is the total wave amplitude and λ the wavelength. The dashed line is the calculated response curve and the arrow on the σ axis indicates the measured frequency of small free oscillations. The symbols represent different total plunger amplitudes: ×, 0·35 cm; ○, 0·60 cm; △, 0·75 cm; ▽, 1·05 cm; ◇, 1·40 cm; □, 1·60 cm.

(ii) When the upper fluid was deep and the lower shallow, the wave profile appeared to be sinusoidal for small amplitudes, but crested upwards when the wave amplitude was sufficiently increased, as shown in figures 4*a*, *b*, *c*, plate 2, and never became flat. Figure 4*b* shows the interface with the second harmonic, as predicted, at a time approximately half way between the times when the displacement was a maximum. Figure 5 is a comparison of the theoretically predicted profile, and that observed in figure 4*a*.

(iii) When the lower fluid was deep and the upper shallow, the wave profile became downward crested at sufficiently large amplitudes (figures 6*a*, *b*, *c*, plate 3, figure 7). The interface was again disturbed by the predicted second harmonic (figure 6*b*), the amplitude of which is in satisfactory agreement with predictions.

(iv) For reasons which are described below, it was not easy to obtain accurate response curves (showing the amplitude of the forced wave for different wave

generator frequencies) and thus the theoretical conclusion (iv) could not be well tested. Response curves which were obtained are shown, figures 8, 9. Figure 8 indicates that in deep water the frequency decreases with increase in wave amplitude, as predicted. The theoretical increase in frequency when the bottom layer was sufficiently small, was not observed at depth to wave-length ratio for the

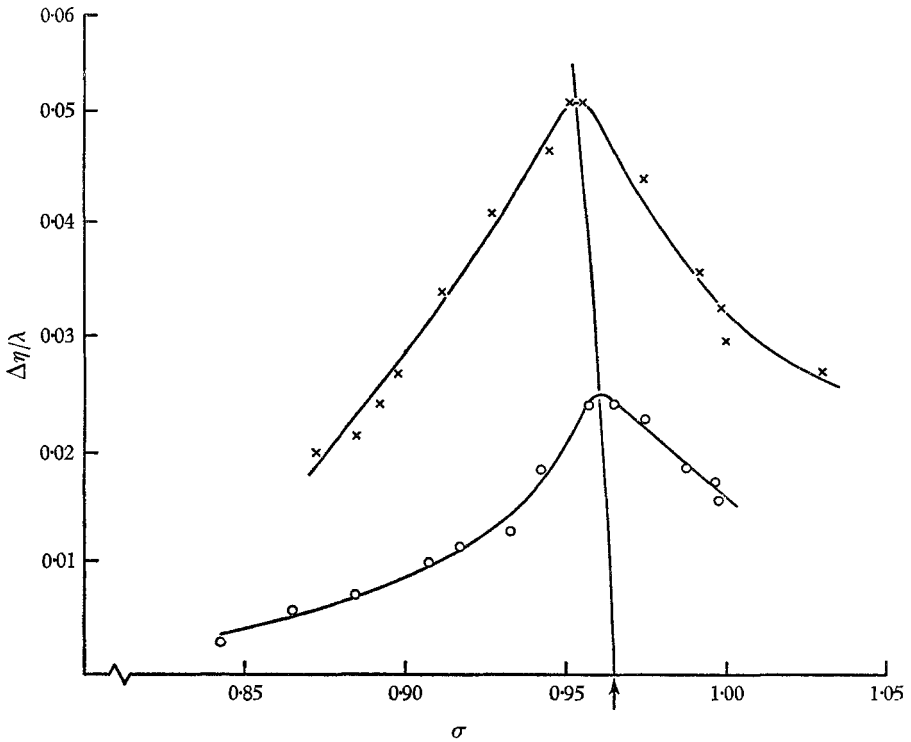

FIGURE 9. Response curves for interfacial waves in a shallow lower fluid, $h_2/\lambda = 0{\cdot}076$, and deep upper fluid, and with density difference $19{\cdot}8 \times 10^{-3}$ g/c.c. The plunger frequency σ is measured in radians per second, $\Delta\eta$ is the total wave amplitude and λ the wavelength. The arrow on the σ axis indicates the measured frequency of small free oscillations. The calculated frequency of small oscillations is 1·025 radians/second. Points ○ represent total plunger amplitudes of 0·40 cm; ×, amplitudes of 0·90 cm.

bottom layer of 0·076, as indicated by figure 9, but the general shapes of the response curves are greatly altered from those in deep water (figure 8). Particularly noticeable is the absence of the steepening on the low frequency side of the peak, which suggests that some alteration in frequency response had taken place. The changes are very similar to those found by Fultz (1962) in his study of surface waves as the fluid depth to wavelength ratio approached the critical value 0·14.

2.3. *The experiments*

The apparatus used in this experiment is shown in figure 10. The apparatus was originally designed for the investigation of standing internal waves in a uniformly stratified fluid, but was found quite suitable for these experiments.

The apparatus consisted of a rectangular tank (A) of depth 30 in., width 14 in. and breadth 8 in., fitted with transparent Perspex walls, (B), at front and back. The side walls were fitted with plungers (C) of height 8 in. and the same breadth as the tank, and the bottom of these plungers was at a distance of 8 in. above the bottom of the tank. Each plunger was moved in and out of the tank in

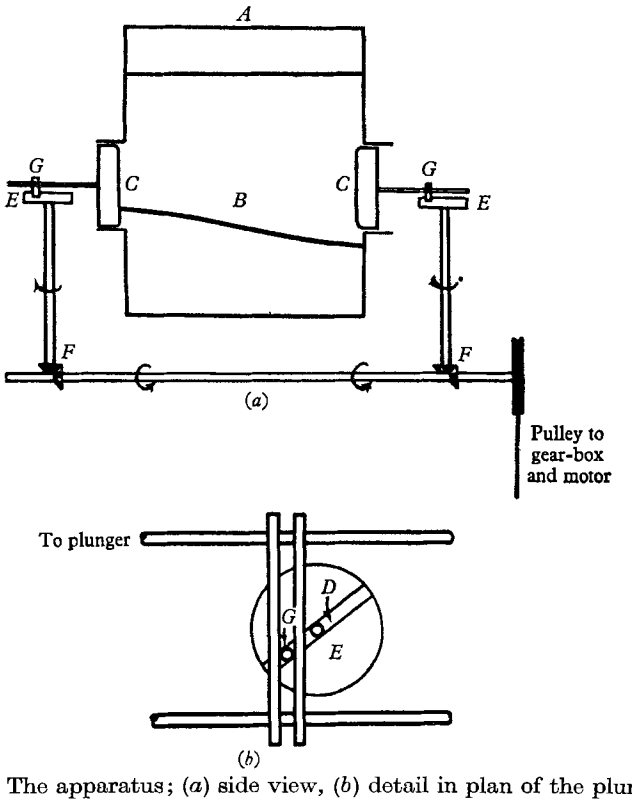

FIGURE 10. The apparatus; (*a*) side view, (*b*) detail in plan of the plunger drive.

simple harmonic motion by the motion of a ball race (G) between parallel rods connected to the plungers. Each ball race was fixed in a diametrical slot of a circular disk (E) which was rotated at constant angular velocity by means of bevelled gears (F) and pulley from a motorized variable speed transmission unit incorporating a further 20–1 gear reduction box. The position of the ball races (G) in the slots of the disks (D) could be varied when the system was at rest, and as a result, the plunger amplitude varied between zero and 5 cm, although in practice 1·6 cm was never exceeded. The plungers could oscillate in or 180° out of phase (the motions being shown in phase by the direction arrows in figure 10). The variation of plunger frequency available was from zero to 0·23 c/s, although the drive was not very stable for frequencies below 0·06 c/s, and in the experiments the variation used was from 0·065 to 0·23 c/s. The mean position of the plungers was adjusted so that, when in this position, the face of each plunger was in the plane of the side wall of the tank. A counter was included in the apparatus so that the number of oscillations of the plungers was automatically recorded.

It had been hoped that it might be possible to seal the area between the sides of the plungers and the tank so that fluid would not escape when the tank was filled, but although several methods were used, it was not found possible to obtain a sufficiently watertight seal. It was therefore necessary to resort to some other method of containing the fluid, and eventually we had the idea of holding the fluid entirely in a rectangular 'bag' made of polythene, which was itself supported by the tank. Polythene had two properties which made it suitable. It was pliable so that the plunger motion was transmitted to the fluid in the 'bag', and it was translucent so that the fluid motion within could be clearly observed and photographed. The 'bags' were made using a heat sealing machine at the Low Temperature Research Station in Cambridge. A large number of 'bags' were eventually made because leaks developed, particularly at the corners which were difficult to seal, usually after the 'bag' had been used two or three times. The lines which occur in some of the photographs are the result of small wrinkles in the polythene when it was pressed by the pressure of the fluid against the Perspex tank walls. These wrinkles were difficult to remove without disturbing the fluid.

The fluids used in all except one of the experiments, were water and brine, one or other being coloured by a little dissolved dye (gentian violet or potassium permanganate) to make the interface visible. When filling, the tank was first filled to a predetermined level with water, and then the heavier brine slowly added from a tank through a vertical tube to which was fixed a horizontal plate which rested on small supports on the bottom of the tank; the bottom of the tank deflected the flow horizontally and the plate reduced mixing. The filling tube was made of glass and is visible in some of the photographs. It was held against a wall, usually in the appropriate position of the wave crest, where horizontal fluid motions are small, and did not appear to disturb the interface in its vicinity in any of the experiments. The amount of dynamic mixing occasioned by this method of filling was small, and sharp interfaces were observed between the dye and the clear fluid. The amount of diffusive mixing was probably larger. The diffusion of salt from the brine across the interface by molecular processes during the time of filling would result in a layer of gradually changing density between the two fluids with a scale of thickness of $2(K_s T)^{\frac{1}{2}}$ where K_s is the molecular diffusivity of salt ($1{\cdot}4 \times 10^{-5}$ cm^2 s^{-1} at 20 °C) and T is the time of filling, usually between 1 and 2 h. Thus the thickness of the interface might be expected to be of the order of 0·6 cm. The effect of this on the wave frequency is discussed later. The dynamic mixing of the interface is indicated by the appearance and motion of the upper surface of the dyed region. Diffusive mixing of the salt at the interface is not so indicated, and in this case the top of the dyed region coincides with the mean density level, if the diffusivity of the dye is much less than that of salt.† In the mixing processes by breaking described later, the motion of the upper surface of the dye will represent the motion of the mean interface.

The undisturbed interface was usually arranged to lie level with the bottom of

† No measurements of the molecular diffusivities in water of the dyes used have been found in the literature. Stearn, Irish & Eyring (1940) quote the range of diffusivities of various dyes as $0{\cdot}17 \times 10^{-5}$ to $0{\cdot}58 \times 10^{-5}$ cm^{2}s^{-1}, somewhat less than that of salt.

the plungers so that the mean level of the interface in the wave motion did not move vertically even when the plungers moved in opposition (180° out of phase).† A false bottom was added to the tank when studying interfacial waves with a shallow lower fluid.

The densities of the two fluids were measured in two ways, the first by means of a salinometer calibrated for density and incorporating a temperature correction and the second by means of a density bottle. The results obtained by the two methods were substantially in agreement.

The frequency of the plungers was found by timing oscillations with a stop watch. The wave amplitudes were measured directly against a vertical rule, the motions being so slow that sufficient time was available to measure, after some practice, the distance between crest and trough to within a millimeter.

Experiments were first tried with one plunger working alone, when both fluids were deep and the plunger amplitude was quite large, 1·6 cm. As the frequency of the plunger was gradually increased, successive forms of the interfacial wave displacement were observed as the wavelength of the disturbance decreased through the values $2W/n$ ($n = 1, 2, 3, \ldots$), where W is the distance between the side walls of the tank, and n is an integer which we shall refer to as the modal number, to define the shape of the waves observed. The amplitudes and phases of the oscillation were much as those found by Taylor (1953) in the study of surface standing waves. When the plunger motion was first started at some low frequency, the amplitude of the wave motion at the interface gradually increased, reached a maximum, and then oscillated slightly before reaching a constant value with the appearance of the mode $n = 1$. When the frequency was now increased slightly, the amplitude of the wave increased. This increase of amplitude with the frequency continued until the frequency reached a critical response value, when the phase of the wave relative to the plunger changed by 180°. This phase change took a number of oscillations to complete, and for a time the wave motion remained 90° out of phase with the plungers. This change of phase was also accompanied by an increase in amplitude. If the plunger motion was stopped at this stage the wave motion continued for some time before dying out. Further increases in frequency caused a decrease in wave amplitude and a gradual change in form of the profile until it resembled the mode $n = 2$ with one complete wave length across the tank. Further increase in frequency then caused in succession, increase in amplitude until a change of phase of 180°, decrease, gradual change to the profile of mode $n = 3$, and then again increase in amplitude, the stages being repeated. It was found possible to distinguish the mode $n = 4$ and with care even higher modes might have been obtained.

When both plungers were used moving in opposition it was not found possible to generate the odd modes; only the odd modes could be generated when the plungers moved in phase. A small vertical motion of the free surface was occa-

† It was found impractical to observe and generate waves in this way when the upper fluid was shallow, because very large plunger amplitudes were necessary to excite the waves. When experimenting with a shallow upper fluid the undisturbed interface was arranged to lie level with the top of the plungers, resulting in a mean displacement of the interface which had to be taken into account when the plungers moved in opposition.

sioned when the plungers moved in opposition, but this did not seem to affect the motion or the profile of the interface. No wave form was ever visible on the free surface, and, so far as could be seen it remained undisturbed in spite of the sometimes violent internal motions at the interface. The effects on the wave profiles of frequency increase with two plungers was substantially as described for the single plunger but with the relevant modes absent.

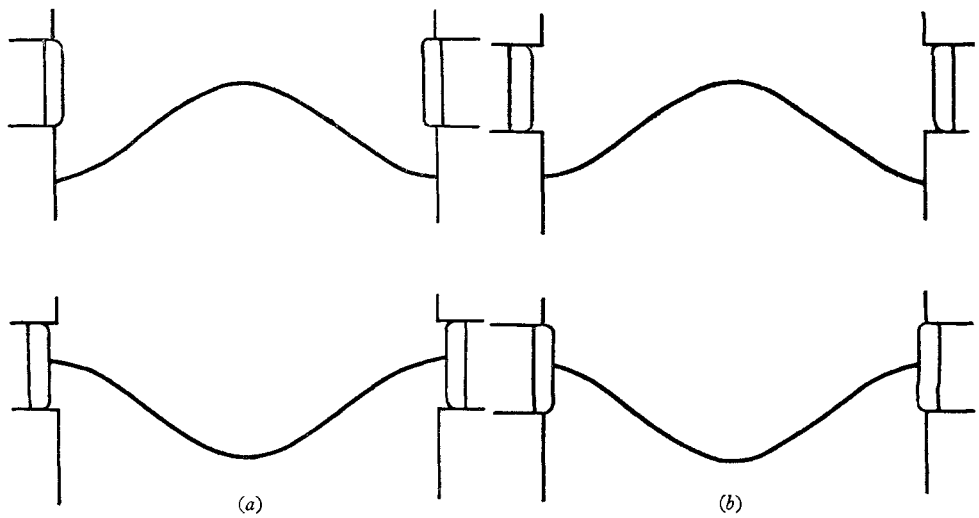

FIGURE 11. Sketch showing the relationship between the phases of waves and plungers. (*A*) plunger frequency greater than the natural wave frequency. (*B*) plunger frequency less than the natural wave frequency.

The majority of experiments were carried out with the two plungers working in opposition using the second mode. The phases of the waves relative the the plungers in the experiments when both fluids were deep or the lower shallow, are shown in figure 11. (The phases when the upper fluid was shallow and the interface level with the top of the plungers, were 180° different from those shown in figure 11.) Figures 2, 4 and 6 mentioned in §2.2 were obtained by oscillating the plungers a few times near the critical frequencies already determined by earlier experiment, then stopping the plunger motion and photographing after the generated wave had oscillated four or five times. (In shallow water damping was large, and the photographs were taken with the plungers oscillating at the critical frequency.) The waves so created were gradually damped.

For the mode $n = 2$ in deep water with a density difference between the fluids of 0·01 g/c.c. and a starting total amplitude of 2 cm, the waves could be distinguished for 4 or 5 min, i.e. for about 30 oscillations, before they were damped out. The waves could usually be detected until their amplitude was about 0·1 cm and these observations led to an estimated damping coefficient, $q \doteqdot 0{\cdot}01\ \mathrm{s}^{-1}$.† The damping was found to be greatly increased when the depth of one of the fluids was small compared to the wavelength. It also increased as the modal number increased, or as the wavelength decreased. These findings are

† The time dependence of all first-order variables is $\sin(\sigma t + \delta)\, e^{-qt}$ where δ is a constant.

in agreement with the predictions of Harrison (1908). A discussion of the effects of viscosity is included in appendix 2.

When working with deep fluids of varying density differences, it was discovered that the maximum wave amplitude which might be obtained at a fixed plunger amplitude increased as the density difference between the fluids increased. This is clearly shown in the response curves for fixed plunger amplitude, figure 12. The curves are drawn for wave oscillation in mode $n = 2$ at a total plunger amplitude of 0·35 cm and varying density differences. This effect is referred to in appendix 2.

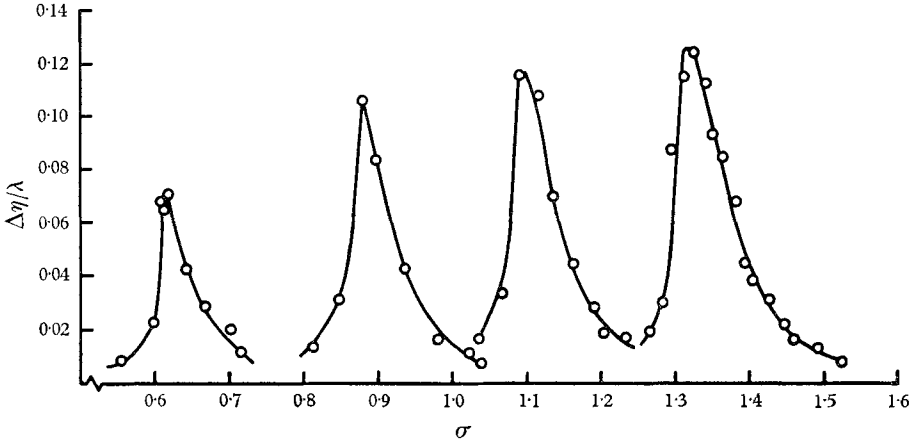

FIGURE 12. Response curves for different density differences and constant total plunger amplitude 0·35 cm. Total wave amplitude, $\Delta\eta$, divided by wavelength, λ, is plotted against plunger frequency σ measured in radians per second. The curves from left to right are for density differences of 4·7, 10·0, 15·0 and 22·8, 10^{-3} g/c.c. respectively.

Wave breaking: observations

When the two plungers were used and both fluids were deep, it was found that at a sufficiently large plunger amplitude near the critical frequencies, irregularities occurred in the wave profile near the modes. The form of the irregularity may be seen in figure 13, plates 4 and 5. The appearance of the irregularity was similar to that which might be envisaged by a vortex of varying sense lying in the interface perpendicular to the plane of motion. As the crest of the wave rose up, the interface near the mode sheared into the position shown in figure 14 (as if a vortex of right-handed sense had been applied at the node at the right of the crest, or a left-handed vortex at the left node). As the crest collapsed, mixing occurred in the region of the nodes, the interface became almost flat and then sheared in the opposite sense in the trough. Careful examination revealed that the wave profile became blurred at the nodes at smaller amplitudes than those at which the overturning described above took place, and the effect may be seen in figure 2.

The events leading up to and following the irregularities were as follows. We suppose that the plunger amplitude and frequency were selected as being those which were known from past experience to cause the full sequence of events, and

that the plungers were started from rest. (i) The wave amplitude increased gradually; the profile was symmetrical and sharply defined. (ii) At wave slopes† of about 0·2 blurred regions became apparent near the wave nodes; the remainder of the profile remained sharp. (iii) At wave slopes of about 0·4, the irregularities at the nodes as described above were observed. The interface became gradually less distinct as a result of the mixing in the region of the node. The profile became more grotesque, almost resembling a mushroom shape at times. Qualitatively

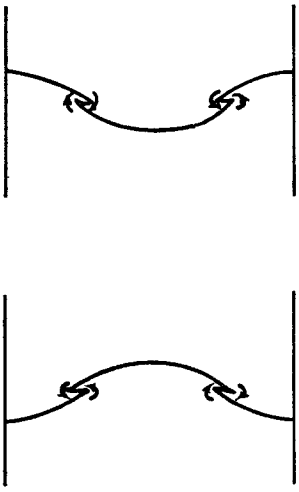

FIGURE 14. The irregularities which occur in the standing wave profile and the suggestion of vortex motion indicated by the arrows.

the same features were observed when the upper, rather than the lower fluid, was coloured. (iv) The two-dimensional motion broke down and cross-waves, with the same frequency and in phase with the plungers occurred. These cross-waves were observed by following the motion of the interface against the side walls of the tank. The displacement could be clearly seen to be a half wavelength. The motions became quite violent at times and streamers of the lower fluid were thrown up into the upper near the walls where the vertical motion was affected by horizontal motion of the plungers. This resulted in mixing. Two different forms of the cross-waves were observed, one in which the interface was twisted, the other in which the whole moved in phase in the cross mode, the former being most usually found. The latter was found to change into a twisting mode on occasions, but the reverse was not observed. The forms of the cross-modes are shown in figures 15 and 16. It is worth comparing these observations of interfacial cross-modes with the surface cross-modes observed by Taylor, and Lin & Howard‡, described in the introduction. The phase and frequency differ in the two cases. The occurrence of a cross-mode is not altogether unexpected, since the

† Wave slope is here taken as $2\pi a/\lambda$, where a is half the total wave amplitude, and λ the wavelength.

‡ The theoretical work of Lin & Howard cannot be extended directly to this model, since an essential part of their analysis was based on wave generation by flaps rather than by plungers.

natural frequency of a transverse mode of wavelength twice the breadth, B, of the tank, is $(\pi g/B)^{\frac{1}{2}}[(\rho_2-\rho_1)/(\rho_1+\rho_2)]^{\frac{1}{2}}$, while the natural frequency of the ordinary wave of mode $n = 2$ is $(2\pi g/w)^{\frac{1}{2}}[(\rho_2-\rho_1)/(\rho_1+\rho_2)]^{\frac{1}{2}}$, where W is the tank width. The ratio of these frequencies, $(w/2B)^{\frac{1}{2}}$ is 0·936 in the experiment, and this is not far from unity.

The times in which the motions persisted in each of the first three stages before transition to the next depended on whether or not the plunger amplitude was sufficient to allow the motion to develop through all the stages, but typically the motion would remain in stage (i) for about 5 oscillations, stage (ii) for 12 oscillations, and stage (iii) for 12 oscillations before stage (iv) was reached. No further development after stage (iv) was observed.

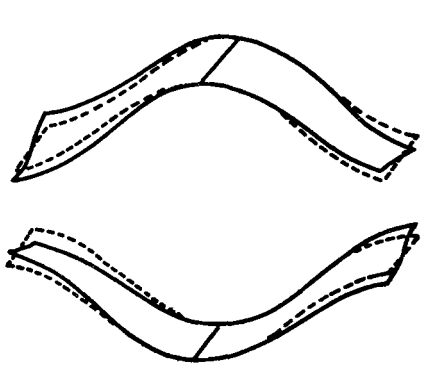

FIGURE 15

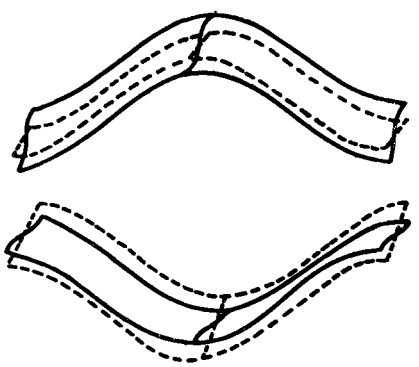

FIGURE 16

FIGURE 15. Cross-waves in the observed twisting form. The continuous lines represent the wave profile, seen in perspective, when the cross waves are present, superimposed on the (dashed) primary, $n = 2$, wave.

FIGURE 16. Cross-waves in the in-phase motion.

If the natural frequency of the wave motion was observed before and after the events described above, by exciting the wave and then timing 20 free oscillations, it was found that the frequency was reduced. For example, on one occasion, when first excited, the wave frequency was 0·83 rad/sec. After 20 oscillations of the plunger in which the wave reached stage (ii) but not stage (iii), the frequency was 0·812 rad/s. After a longer run in which stages (iii) and (iv) were reached and violent motions and mixing occurred, the frequency was found to be 0·76 rad/s. On a few occasions it was found that the result of mixing at stage (iii) was sufficient to change the natural frequency so much that the plunger frequency was no longer close to the natural, and the wave response was therefore less, resulting in reduction in wave amplitude before the cross-mode developed.

In an attempt to observe more clearly the form of the irregularities at the interface, an experiment was made with a layer of dyed fluid of thickness 0·7 cm and density 1·0037 g/c.c. lying between two deep uncoloured layers of densities 0·9978 and 1·0077 g/c.c. The period of free oscillation in mode $n = 2$ was found by oscillating the plungers a few times and timing the resultant oscillation in the

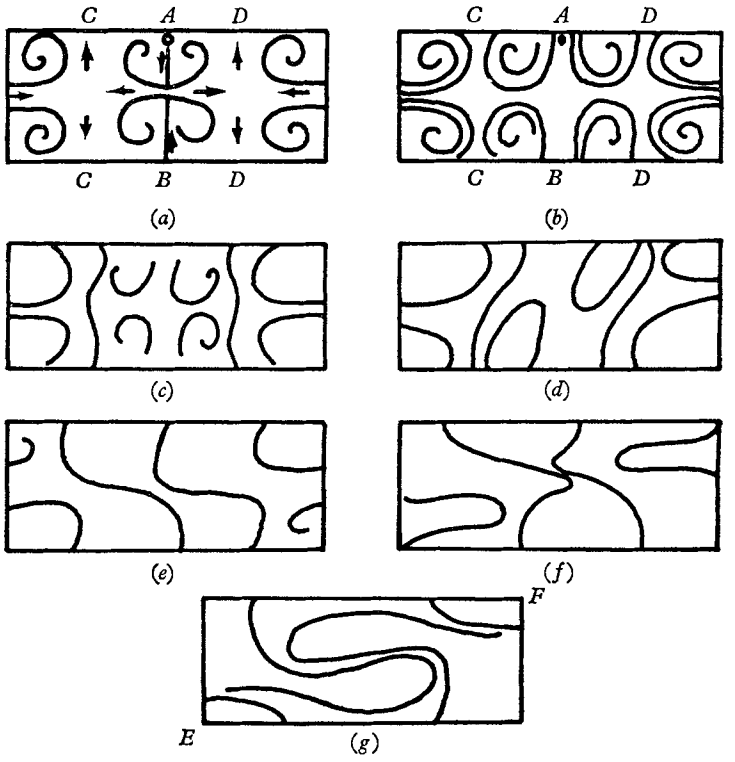

FIGURE 18. Diagrams of stream patterns observed (from above) in a layer of dye lying at the interface between two fluids of different densities when a standing wave is generated. AB is the line of the central antinode, CC and DD the position of the nodes. The circle near A is the position of the filling tube. The development of a cross mode causes the change in the patterns in diagrams (c) to (g).

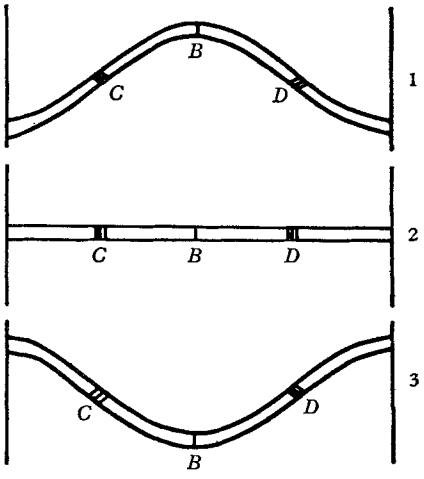

FIGURE 19. Diagrams of the streaks of clear fluid in a dyed layer viewed horizontally. Three positions of the layer are shown. The short lines at the nodes, C and D, and the antinode, B, show the position of the streaks and correspond to those of figure 18b.

fluid, and the plunger frequency was then set close to this frequency of free oscillations. The total wave amplitude grew to 5·2 cm. The thickness of the dyed layer was seen to increase slightly near the nodes, and to assume the shape shown in figure 17, plate 6, at the times of maximum displacement, a shape which resembled that of the irregularities of the two fluid system. In addition to this irregular shape of the profile, streaks of less densely coloured fluid in the vicinity of the wave crest and node were observed. There followed, after a few oscillations, the growth of a cross-mode of the in-phase kind described above, which changed into a twisting cross-mode after 15 or 20 further wave periods.

The experiment was repeated with a coloured layer of density 1·0034 g/c.c. and thickness 0·5 cm separating deep uncoloured layers of densities 0·9982 and 1·0037 g/c.c. During filling it was noticed that streaks of relatively less coloured fluid existed in the dyed layer, when seen from above, and it seemed that they were associated with currents flowing in the lower fluid. The patterns disappeared some time after filling stopped. When the plungers were started the wave amplitude grew, and after seven oscillations had grown to 4·5 cm. At this time a streak pattern of relatively less coloured fluid in the dyed layer was noticed when viewed from above or below. The pattern is shown in figure 18(*a*). The currents associated with the streaks appeared to be away from the wall at the antinodes and towards the nodes in the body of the fluid. Arrows indicating the motions have been drawn in figure 18(*a*). The layer of dyed fluid oscillated up and down with the wave motion, but so far as could be seen, the growth and motions of the streaks continued in the same direction throughout the wave motion and the pattern did not seem to change its form substantially during one oscillation. No wave breaking similar to that described in stage 3 was observed. By the 38th oscillation of the plungers, the streak pattern in the dye had developed into that shown in figure 18(*b*). The appearance of the streaks when viewed horizontally is shown in figure 19, and they resembled the streaks seen in the preceding experiment. By the 88th oscillation the pattern was much as shown in figure 18(*b*), but a small gap had developed along the line AB separating the dyed layer into two parts. The pattern did not change after this and appeared to be steady although the experiment was continued up to 160 oscillations. Photographs of the streaks, taken from an angle below the interface, at the 70th and 131st oscillation are shown (figure 20, plate 7).

The experiment was again repeated with a dyed layer of density 1·0138 g/c.c. and thickness 0·4 cm between deep uncoloured layers of densities 0·9978 and 1·0142 g/c.c. The effects were at first qualitative as in the last experiment, and again no breaking as described in stage (iii) occurred. However, the streak pattern developed differently. The main features are shown in figure 18(*c*) to (*g*). It was found that by the time the pattern had changed into the configuration shown in figure 18(*g*), a twisted cross-mode had developed with resulting maximum wave amplitude at points E and F.

We believe that the streaks are the manifestation of secondary currents at the interface generated in the boundary layers at the vertical walls of the tank, similar to those described by Rayleigh (1896, §§ 260 and 352) in the case of standing sound waves, which produce the piles of dust found in the Kundt's dust-tube

experiment. Similar effects occur in surface standing waves.† A search was made for mean vertical currents generated by small interfacial wave motions by adding aluminium powder to the water and brine and following the motion of the particles, but no evidence of such secondary currents was found. It would perhaps be difficult to identify such mean currents in this way because the time scale of the motion would be large.

In the experiments in which one of the fluids was shallow, the irregularities of stage (iii) were not observed and a direct transition from stage (ii) to stage (iv) followed.

An attempt was made to identify more closely the mechanism leading to the instabilities which produce mixing, by using two immiscible fluids. The fluids used were water and a mixture of carbon tetrachloride and kerosine, the mixture being of density 0·0084 g/c.c. less than that of water. The first observation made when the tank had been filled was that the meniscus at the edge of the interface was very large. (The effect of capillary forces is given by the number, $T/g(\rho_2-\rho_1)L^2$, see, for example, Rosenhead (1963, p. 32) where L is a length scale. The size of the meniscus which might be expected at the interface is therefore $[T_I\rho_2/T(\rho_2-\rho_1)]^{\frac{1}{2}}$ times the meniscus at the water surface, where T_I is the surface tension at the interface, T the air–water surface tension. The surface tension at the interface was estimated at 44 dynes/cm, by measurement of the forces required to lift a light plastic ring off the fluid surfaces, and this would imply a meniscus at the interface about eight times as large as that at an air–water boundary.) Waves of mode $n = 2$ were excited by oscillating the plungers and although there was sometimes evidence at the interface of the presence of small waves of much smaller wavelengths than the width of the tank, these waves were not positively identified with the position of the primary wave node. It was noticed that the waves produced were smaller in amplitude than the waves observed before between brine and water with the same density difference produced in similar circumstances. No evidence of breaking was seen. The experiment was discontinued when it was found that leaks had developed in the apparatus (probably as a result of contact with the mixture) and not repeated because the observations made were not encouraging, mainly because of the large meniscus effect. (Unfortunately the restrictions on the frequency range available limited our experiments to very small density differences, and thus to a large meniscus.)‡

From what has been observed about the mixing and its effects on the natural frequency of the waves, it is clearly impossible to obtain response curves for a two fluid system by simply increasing the frequency by stages through and beyond

† It is possible to detect these currents in surface gravity waves produced in a bucket. A plastic bucket is suitable since the waves may easily be started by slightly vibrating opposite sides of the bucket by hand at a frequency equal to the natural frequency of the waves. If the surface is marked by aluminium powder (soap suds or pepper are equally efficient), motion of the water may be seen in the boundary layers away from the nodes towards the antinodes, and away from the wall at the antinodes themselves. Similar currents are generated in a rectangular container containing water, when it is gently rocked.

‡ For footnote see opposite page.

the critical frequency and measuring the resulting wave amplitudes, for as soon as the amplitude became large enough for stage (ii) to occur, mixing starts and the natural frequency of the waves changes. The magnitude of the changes in frequency occasioned by the mixing are not negligible, as is shown in the example quoted.

Early estimates of the natural frequency of the waves were based on the response curves obtained in the way described above and were found to be 6 or 7 % smaller than those estimated (as found by Schmidt). However, when great care was taken to excite a wave of amplitude not sufficient to reach stage (ii), and also to make the experiment and filling as quickly as possible to reduce molecular diffusion, much closer agreement was found between the observed and theoretical frequencies. For the mode $n = 1$ when both fluids were 19·1 cm deep and the density difference was 0·0204 g/c.c. the observed frequencies from two experiments found by timing 10 oscillations, were 0·8837, 0·8837, 0·8812, 0·8863, 0·8837, 0·8876, the mean 0·8843 rad/s, comparing with 0·8861 found theoretically. The frequencies were not compared for modes and density differences other than those shown in the response curves.

The response curves shown in figure 8, 9 and 12 must be regarded as only approximations to the exact curves which might be obtained for two fluids with a sharp interface between them. Each curve was obtained in two parts and in two separate experiments, the first by approaching the natural wave frequency from above and the second by approaching from below, so as to reduce the amount of mixing which had taken place in reaching any wave response amplitude at a given frequency. Moreover, the selected plunger frequencies at which the wave amplitudes were measured were few, and the times taken in obtaining the frequencies and the corresponding amplitudes were made as short as possible, while allowing the wave amplitude to develop fully and the frequency to be carefully measured, again so as to reduce the amount of mixing. (In fact the wave amplitude was measured after about 12 oscillations at each frequency.) The measurements of frequency were correct to about 0·3 %. In spite of these arrangements, there was evidence that some mixing had occurred, particularly when the wave amplitudes became large, and the response curves are substantially removed from the theoretical.

2.4. *Wave breaking: discussion*

While it has not been found possible to construct a complete stability analysis for the standing interfacial wave, the general dynamics of the wave breaking

‡ Dr Brooke Benjamin has kindly drawn my attention to a dissertation by Carstens (1964) in which this experiment with immiscible fluids is described. The observations of short wave-length disturbances (which ultimately break and eject globes of the upper fluid into the lower, and globes of lower fluid into the upper) at the nodes of the standing wave are particularly interesting. The stability problem in that experiment differs from the present problem in that surface tension provides a stabilizing force at the interface and a threshold of instability (a minimum shear for which a disturbance may be amplified) may be found. Carstens also observed the existence of the secondary currents at the interface.

seems to be quite clear. It is found that the wave crests and troughs, in contrast to the surface standing wave crests, are flat, indeed markedly so, and no instability appears to be associated with this region. As noted by Phillips (1966, p. 186) and others, it is only when local accelerations in the wave motion become comparable with the acceleration due to gravity (and not the reduced gravity) that the Rayleigh–Taylor type of instabilities may occur; and while such accelerations are possible in the surface standing wave at its crest (and do lead to breaking as found by Taylor), they are not likely to be found in internal gravity waves. To first order, the fluid acceleration reaches a maximum value at the wave crest of $a\sigma^2$, which is equal to $akg(\rho_2-\rho_1)/(\rho_1+\rho_2)$ when both fluids are deep. Even for large wave slopes, ak, this acceleration is generally much less than g in naturally occurring phenomena, and, in particular, is always much less in our experiments. Another mechanism must therefore be present to explain the observed instability at the node of the interfacial wave, the part of the wave where, significantly, the local shear at the interface resulting from the wave motion itself, is greatest. It is suggested that this instability is a shear instability, although not in its most simple form, for the local shears at the interface are periodic in both space and time and the interface itself does not remain horizontal. A mark of this complexity is the observation that a single roll (or 'vortex') is generated at the wave node, and not a small group of waves or rolls as might be expected if some locally uniform conditions were present at the wave node. It is relevant to mention that in the case of the two-fluid Rayleigh–Taylor instability, which in many ways resembles the situation under discussion here, Daly (1967) has recently established the existence of a single 'vortex' or roll at the interface in the finite amplitude motion for sufficiently small differences in density between the two fluids and has ascribed the generation of the roll to the Kelvin–Helmhotz instability.

While the roll which develops in our experiments is very similar to that found by Daly, in practice it is impossible to establish an interface between two miscible fluids in which the density gradient is discontinuous in a mathematical sense. In fact it is possible to estimate a Richardson number, Ri associated with the maximum local shear at the interface at the onset of the observed wave irregularities, based on the observed wave slopes, wavelengths and the thickness of the interface, on the assumption that the fluid velocities are just those predicted by the theory for two deep fluids. When breaking (stage ii) is first observed, the value of Ri is estimated to be about 0·36; stage (iii) is reached at a Richardson number of about 0·01. The theoretical analysis of the situation is not complete.

Yet to be explained completely is the observed 'blurring' of the interface (stage ii) which precedes 'roll-up' (stage iii). It was first thought that this might be the effect of secondary currents associated with the primary wave motion carrying fluid of intermediate density to the region of the wave node, but more recent observations of instability in heterogeneous shear flow in a slightly tilted tube† suggest that the 'blurring' is associated with the development of the

† An account of these experiments was presented at the International Conference on Stratified Fluids at Ann Arbor in April 1967, and further results will be published in a later paper.

instability itself and not with the primary wave motion. It is expected that better estimates of the Richardson number at which instability is first observed may be deduced from these further experiments.

3. Standing internal waves in a continuously stratified fluid

3.1. *General theory*

We wish to find a periodic standing wave solution of the equations governing the two-dimensional motion between two vertical walls of an inviscid, incompressible fluid, which is continuously and stably stratified. The lower boundary of the fluid is supposed to be horizontal and rigid; the upper boundary will also be fixed horizontally although in general an extension to include a free upper boundary may be possible.

The method used will be seen to be akin to that already applied to progressive internal waves (Thorpe 1968), but is really an extension of the method of solution applied to surface waves by Penney & Price. Implicit in our assumptions is that certain series in powers of wave amplitude do converge for sufficiently small amplitudes. The solution of standing wave problems is easier than that of problems involving progressive waves since more boundary conditions (those at vertical walls) are specified, and there is no difficulty in matching given upstream conditions or in defining a perturbation about a given state. We shall consider first the general problem, that of waves in a fluid which, in the absence of waves, has a density $\hat{\rho}_0(\hat{z})$, where axes $\hat{x}, \hat{z}$, are taken horizontally and vertically respectively and ($\hat{}$) represents a dimensional quantity. If $\hat{\eta}(\hat{x}, \hat{z}_0, \hat{t})$ is the displacement of a particle of density $\hat{\rho}_0(\hat{z}_0)$ from its original position $\hat{z}_0$, then since there is no exchange of fluid across the vertical walls or horizontal bottom of the containing boundary, by continuity the fluid initially lying below a line of particles $\hat{\eta}(\hat{x}, \hat{z}_0, \hat{t})$ remains below, and hence the mean value of $\hat{\eta}$ with respect to $\hat{x}$ is zero. This condition will be used to specify certain functions in the later analysis.

The fluid is incompressible and we may therefore define a stream function $\hat{\psi}(\hat{x}, \hat{z}, \hat{t})$ such that horizontal and vertical velocity components $(\hat{u}, \hat{w})$ of fluid velocity are

$$\hat{u} = \partial\hat{\psi}/\partial\hat{z}, \quad \hat{w} = -\partial\hat{\psi}/\partial\hat{x}. \tag{3.1.1}$$

We shall find it convenient to make the Boussinesq approximation. By doing so we may restrict the application of the analysis to certain scales of motion, just as was found for progressive waves. The validity of the Boussinesq approximation has been examined in some detail in the progressive wave theory (Thorpe 1968) and the restrictions of the application of this analysis are exactly as found there. Broadly the restriction is to medium scales of motion and theory is not applicable to long-standing waves in the larger lakes.

The vorticity equation and the equation of continuity become

$$\hat{\rho}_0(0)\left[\frac{\partial}{\partial\hat{t}}\hat{\nabla}^2\hat{\psi} + \hat{J}(\hat{\nabla}^2\hat{\psi}, \hat{\psi})\right] = \hat{g}\frac{\partial\hat{\rho}}{\partial\hat{x}}, \tag{3.1.2}$$

and

$$(\partial\hat{\rho}/\partial\hat{t}) + J(\hat{\rho}, \hat{\psi}) = 0, \tag{3.1.3}$$

where $\hat{\rho}(\hat{x},\hat{z},\hat{t})$ is the fluid density in the wave motion, and J is the Jacobian. We shall take the fixed boundaries at $\hat{x}=0,\hat{W}$ where $\hat{u}=\partial\hat{\psi}/\partial\hat{z}=0$, and at $\hat{z}=0,\hat{H}$ where $\hat{w}=-\partial\hat{\psi}/\partial\hat{x}=0$. The case when $\hat{H}$ is infinite may be included.

We now non-dimensionalize the equations using the width, $\hat{W}$, the density, $\hat{\rho}_0(0)$, and the acceleration due to gravity, $\hat{g}$. Then (3.1.2) and (4.1.3) become

$$\frac{\partial}{\partial t}\nabla^2\psi+J(\nabla^2\psi,\psi)=\frac{\partial\rho}{\partial x} \tag{3.1.4}$$

and

$$(\partial\rho/\partial t)+J(\rho,\psi)=0, \tag{3.1.5}$$

and the boundary conditions are

$$\partial\psi/\partial z=0 \quad \text{at} \quad x=0,\pi, \tag{3.1.6}$$

and

$$\partial\psi/\partial x=0 \quad \text{at} \quad z=0,\pi/r, \tag{3.1.7}$$

where

$$x=\pi\hat{x}/\hat{W}, \quad z=\pi\hat{z}/\hat{W}, \quad t=(\hat{g}\pi/\hat{W})\hat{t},$$

$$\psi=(\pi^3/\hat{g}\hat{W}^3)^{\frac{1}{2}}\hat{\psi}, \quad \rho=\hat{\rho}/\hat{\rho}_0(0), \quad J(\rho,\psi)\equiv\partial(\rho,\psi)/\partial(x,z),$$

and $r=\hat{W}/\hat{H}$. The non-dimensional density of the disturbed fluid is

$$\Pi(z)=\hat{\rho}_0(\hat{z})/\hat{\rho}_0(0).$$

To solve these equations subject to the given boundary conditions and the condition of continuity described above, we make certain further assumptions. We suppose that the stream function is of the form

$$\psi(x,z,t)=\sum_{n=1}^{\infty}\psi_n(z,t)\sin npx \tag{3.1.8}$$

where n and p are positive integers (this satisfies (3.1.7)) and it follows from (3.1.4) and (3.1.5) that the density must be of the form

$$\rho(x,z,t)=\sum_{n=0}^{\infty}\rho_n(z,t)\cos npx. \tag{3.1.9}$$

(This assumption is similar to that of Penney & Price although here the dependence of ψ_n on z does not follow automatically, since ψ satisfies a more complicated equation than the Laplace equation satisfied by the stream function in the homogeneous fluid.)

Substitution of these expressions (3.1.8), (3.1.9), leads to the following, somewhat involved, expressions:

$$\begin{aligned}\sum_{n=1}^{\infty}((\psi_n)_{zzt}-n^2p^2(\psi_n)_t+np\rho_n)\sin npx\\ +\left(\sum_{n=1}^{\infty}(\psi_n)_z\sin npx\right)\left[\sum_{m=1}^{\infty}mp((\psi_m)_{zz}-m^2\psi_m)\cos mx\right]\\ -\left(\sum_{n=1}^{\infty}n\psi_n\cos nx\right)\left[\sum_{m=1}^{\infty}((\psi_m)_{zzz}-m^2(\psi_m)_z)\sin mx\right]=0\end{aligned} \tag{3.1.10}$$

and

$$\begin{aligned}\sum_{n=0}^{\infty}(\rho_n)_t\cos npx-\left(\sum_{n=1}^{\infty}(\psi_n)_z\sin npx\right)\left(\sum_{m=0}^{\infty}\rho_m mp\sin mpx\right)\\ -\left(\sum_{n=1}^{\infty}\psi_n np\cos npx\right)\left(\sum_{m=0}^{\infty}(\rho_m)_z\cos mpx\right)=0,\end{aligned} \tag{3.1.11}$$

where $(\psi_n)_z \equiv \partial\psi_n/\partial z$, etc. To proceed further, it is necessary to make some appropriate assumption about the order of magnitude of the terms ψ_n and ρ_n which appear in these equations. The boundary conditions do not impose any scale on ψ (and indeed the magnitude is dependent on the wave amplitude, about which we have made no assumption so far), although ρ must be of order unity, representing the initial density when the disturbance becomes very small. We therefore suppose (and find *a posteriori* that it is consistent) that ψ is small and of order α, where this is a parameter which will be defined in terms of the wave amplitude and fluid depth. The density, ρ_0, is of order unity, and ρ_1 of order α, which follows from (3.1.13) below. Now comparison of coefficients of $\sin npx$ or $\cos npx$ in (3.1.10), (3.1.11), leads to a series of equations in the ψ_n and ρ_n. Moreover, comparing coefficients for $0 \leqslant n \leqslant N$ leads to $2N+1$ equations for $\psi_1, \psi_2, \ldots, \psi_N$ and $\rho_0, \rho_1, \ldots, \rho_N$; an expansion to order N may be solved in closed form. Examination of these equations shows that on the basis of the ordering system defined above, ψ_n and ρ_n are of order α^2. We are thus left with a sequence of equations for ψ_n and ρ_n as functions of time, and z only. The equation at zeroth order is simply

$$(\rho_0)_t = 0. \tag{3.1.12}$$

Hence to zeroth order $\rho_0 = \Pi(z)$, the undisturbed fluid density. The equations at first order are

$$(\psi_1)_{zzt} - p^2(\psi_1)_t + \rho_1 = 0 \tag{3.1.13}$$

$$\rho_{0,t} = 0 \tag{3.1.14}$$

and

$$(\rho_1)_t - (\rho_0)_z\, p\psi_1 = 0. \tag{3.1.15}$$

The term $(\rho_0)_z$ which appears in (3.1.15) is expanded to zeroth order only, since we have assumed that ψ_1 is first order, and so we may replace ρ_0 by $\Pi(z)$ in this equation, and then eliminate ρ_1 from (3.1.13) and (3.1.15) to obtain

$$(\psi_1)_{zztt} - p^2(\psi_1)_{tt} + p^2\Pi'\psi_1 = 0, \tag{3.1.16}$$

where

$$\Pi' \equiv d\Pi/dz.$$

The boundary conditions on ψ_1 are that $\psi_1 = 0$ at $z = 0, \pi/r$. We are seeking a solution which is periodic in time. Suppose that, to first order

$$\psi_1 = \Psi(z)\sin\sigma t, \tag{3.1.17}$$

where

$$(\Psi)_{zz} - p^2(1+\Pi')\sigma^2\Psi = 0; \Psi(0) = \Psi(\pi/r) = 0. \tag{3.1.18}$$

The solutions of this equation are well known and have been discussed by Yih (1960). By implication the horizontal wavelength of the oscillation is $(2/p)$ times the width of the tank, $\hat{W}$. We assume that this wavelength, and therefore the integer p, is given; (3.1.18) is then an equation of standard Sturm–Liouville type and there exists an infinite sequence of positive eigenvalues $\{1/\sigma^2\}$ whose only limit point is $+\infty$ (Yih 1960). We let $\{\Psi_n\}$ be the complete set of corresponding orthogonal eigenfunctions. These different eigenfunctions correspond to different modes of the system. We shall restrict our attention to one of these which has eignfunction Ψ, say, and corresponding eignvalue $1/\sigma^2$ so that

$$\psi_1 = \alpha\Psi(z)\sin\sigma t.$$

From (3.1.13) it follows that

$$\rho_1 = -(\alpha p \Pi'/\sigma)\Psi \cos \sigma t$$

and from (3.1.14) $\rho_0 = \Pi(z) + \alpha f_1(z)$,

where $f_1(z)$ is of zeroth order.

Now suppose that a fluid particle initially at height z and therefore having density $\Pi(z)$, is moved by the wave motion to $z + \eta(x, x, t)$. The density remains unchanged so that

$$\Pi(z) = \rho(x, z+\eta(x,z,t), t) = \rho_0(z+\eta, t) + \rho_1(z+\eta, t)\cos px \tag{3.1.19}$$

expanding to first order. Substituting the known first-order values of ρ_0 and ρ_1 and expanding in Taylor series about z we find

$$\begin{aligned}\eta\Pi' + \tfrac{1}{2}\eta^2\Pi'' + \ldots + \alpha(f_1(z) + \eta f_1'(z) + \ldots) \\ -(\alpha p/\sigma)(\Pi' + \eta\Pi'' + \ldots)(\Psi + \eta\Psi' + \ldots)\cos\sigma t \cos px = 0,\end{aligned} \tag{3.1.20}$$

and hence η is of order α, and, expanding to order α, we have

$$\Pi'\eta = -\alpha[f_1(z) - (p/\sigma)\Pi'\Psi \cos\sigma t \cos px]. \tag{3.1.21}$$

But as we have already remarked the mean value of η with respect to x is zero, and so $f_1(z) = 0$ and to first order we have

$$\left.\begin{aligned}\rho_0 &= \Pi, \\ \rho_1 &= -(\alpha p \Pi'/\sigma)\Psi \cos\sigma t, \\ \psi_1 &= \alpha\Psi \sin\sigma t, \\ \eta &= (\alpha p/\sigma)\Psi \cos\sigma t \cos px.\end{aligned}\right\} \tag{3.1.22}$$

The wave amplitude as a function of z is given by $\alpha p\Psi(z)/\sigma$. As postulated, α is associated with the wave amplitude. In particular cases it may be helpful to specify the maximum amplitude of the wave (that of the maximum fluid displacement in the system), but at the moment we retain the expressions as they stand, and return to (3.1.10) and (3.1.11) to expand to second order. Comparing coefficients we find that

$$(\psi_1)_{zzt} - p^2(\psi_1)_t + p\rho_1 = 0, \tag{3.1.23}$$

$$\begin{aligned}(\psi_2)_{zzt} - 4p^2(\psi_2)_t + 2p\rho_2 \\ = \tfrac{1}{2}p[\psi_1((\psi_1)_{zz} - p^2\psi_1)_z - (\psi_1)_z((\psi_1)_{zz} - p^2\psi_1)],\end{aligned} \tag{3.1.24}$$

$$\rho_{0,t} = \tfrac{1}{2}p(\rho_1\psi_1)_z, \tag{3.1.25}$$

$$(\rho_1)_t - (\rho_0)_z p\psi_1 = 0 \tag{3.1.26}$$

and

$$(\rho_2)_t - 2(\rho_0)_z\psi_2 = \tfrac{1}{2}p[\psi_1(\rho_1)_z - (\psi_1)_z\rho_1], \tag{3.1.27}$$

correct to second order. These equations are solved using the known first-order solution (3.1.22). Since ψ_1 and ρ_1 are known to be first order, (3.1.25) is an equation for the second-order terms which arise in ρ_0. This term is already known to contain no first-order terms, and so (3.1.23) and (3.1.26), equations identical to (3.1.13) and (3.1.15) found earlier, are satisfied by the first-order density and stream function, ρ_1, and ψ_1. Equations (3.1.24) and (3.1.27) express the fact that both ρ_2 and ψ_2 are second order, being represented by products of the first-order terms ρ_1 and ψ_1.

Substituting for ψ_1 and ρ_1 from (3.1.22) into (3.1.25),

$$\rho_{0,t} = -(\alpha^2 p^2/4\sigma)[\Pi'\Psi^2]' \sin 2\sigma t,$$

and integrating,

$$\rho_0 = (\alpha^2 p^2/8\sigma^2)[\Pi'\Psi^2]' \cos 2\sigma t + \alpha^2 f_2(z) + \Pi(z), \tag{3.1.28}$$

where $f_2(z)$ is a function of z of order unity.† On substitution (3.1.24) and (3.1.27) become

$$(\psi_2)_{zzt} - 4p^2(\psi_2)_t + 2p\rho_2 = \tfrac{1}{2}(\alpha^2 p^3/\sigma^2)\,\Pi''\Psi^2 \sin^2 \sigma t \tag{3.1.29}$$

and

$$(\rho_2)_t - 2\Pi'\psi_2 = -(\alpha^2 p^2/4\sigma)\,\Pi''\Psi^2 \sin 2\sigma t. \tag{3.1.30}$$

Eliminating $(\rho_2)_t$ from these two equations we have

$$(\psi_2)_{zzt} - 4p^2(\psi_2)_{tt} + 4\Pi' p^2 \psi_2 = (\alpha^2 p^3/\sigma)\,\Pi''\Psi^2 \sin 2\sigma t. \tag{3.1.31}$$

We look now for a solution of the form $\psi_2 = \Phi \sin 2\sigma t$, where Φ now satisfies

$$\Phi'' - 4p^2\Phi - \frac{\Pi' p^2}{\sigma^2}\Phi = -\frac{\alpha^2 p^3}{4\sigma^3}\Pi''\Psi^2, \tag{3.1.32}$$

subject to the boundary conditions $\Phi = 0$ at $z = 0$ and π/r, and define a set $\{\phi_n\}$ of eigenfunctions of the equation $\phi'' - 4p^2\phi - 4(\Pi' p^2/\sigma^2)\phi = 0$ with boundary conditions $\phi = 0$ at $z = 0$ and π/r, and corresponding eigenvalues $\{1/\sigma_n^2\}$, so that

$$\phi_n'' - 4p^2\phi_n - (4\Pi'/\sigma_n^2)p^2\phi_n = 0, \quad \phi_n = 0 \quad \text{at} \quad z = 0, \quad \pi/r. \tag{3.1.33}$$

The set $\{\phi_n\}$ is complete and orthogonal in the sense that

$$\int_0^{\pi/r} \Pi'\phi_n\phi_m\,dz = 0 \quad (n \neq m),$$

and the infinite sequence of eigenvalues is positive with only limit point $+\infty$. If now we let

$$\sum_{n=1}^{\infty} a_n\phi_n = \Psi^2\Pi''/\Pi',$$

where

$$a_n = \frac{\int_0^{\pi/r} \Psi^2\Pi''\phi_n\,dz}{\int_0^{\pi/r} \Pi'\phi_n^2\,dz}, \quad \text{and} \quad \Phi = \alpha^2 \sum_{n=1}^{\infty} b_n\phi_n,$$

substitution into (3.1.32) gives

$$b_n = \frac{p a_n \sigma_n^2}{4\sigma(\sigma_n^2 - 4\sigma^2)}, \tag{3.1.34}$$

† If continuing the expansion to any higher order, we must regard σ as a parameter which may also be expanded as a series in powers of α,

$$\sigma = \sum_{n=0}^{\infty} \alpha^n \omega_n,$$

with ω_0 identified as the eigenvalue σ of (3.1.18). The correction, ω_1, to this eigenvalue is determined in the second-order analysis, but is identically zero. In the expansion to third order in the particular case

$$\Pi(z) = 1 - \mu z$$

discussed below, the variation due to finite wave amplitude is found, but the details of solution are omitted. The technique of varying σ is standard and well known in the case of surface waves; it is no more complicated here.

provided that $\sigma_n^2 \neq 4\sigma^2$ if $a_n \neq 0$. Failure of the standard theory at these frequencies has similarly been found in the analysis of surface standing waves by Tadjbakhsh & Keller (1960) and Concus (1962, 1964), although experiments have not revealed any extraordinary behaviour at these frequencies. (If we write $\sigma_n = \sigma_n(2p)$, the eigenvalue of (3.1.33), then σ is one of the set $\{\sigma_m(p)\}$ and the theory fails when $\sigma_n(2p) = 2\sigma_m(p)$ for a given m, and n such that $a_n \neq 0$. It appears that in this case there will be a resonant interaction between the second harmonic of the primary wave and another free mode of oscillation of the system).

In general, however, $\sigma_n^2 \neq 4\sigma^2$, and

$$\psi_2 = \frac{\alpha^2 p}{4\sigma} \sum_{n=1}^{\infty} \frac{\sigma_n^2}{\sigma_n^2 - 4\sigma^2} a_n \phi_n \sin 2\sigma t. \tag{3.1.35}$$

Since $\Sigma a_n \phi_n$ is, by definition, convergent, and $\{1/\sigma_n^2\}$ is an infinite sequence of positive eigenvalues with only limit point $+\infty$, it follows that

$$\sum_{n=1}^{\infty} [\sigma_n^2/(\sigma_n^2 - 4\sigma^2)] a_n \phi_n$$

is convergent. Clearly other solutions of (3.1.31) may be found, but these correspond to free waves in the system; our attention is now confined to those second-order waves forced by the presence of the first-order wave.

From (3.1.29) and (3.1.33) we have

$$\rho_2 = \frac{1}{8} \frac{p^2\alpha^2}{\sigma^2} \Pi'' \Psi^2 - \left[\frac{\alpha^2 p^2 \Pi''}{8\sigma^2} \Psi^2 + p^2\alpha^2 \sum_{n=1}^{\infty} \frac{a_n \Pi'}{\sigma_n^2 - 4\sigma^2} \phi_n \right] \cos 2\sigma t.$$

The second-order particle displacement, η, may now be found using an expression similar to (3.1.20), and f_2 found from the continuity equation. Omitting the details of the algebra we find in summary that to second order

$$\psi = \alpha \Psi \sin \sigma t \sin px + \frac{\alpha^2 p}{4\sigma} \sum_{n=1}^{\infty} \frac{\sigma_n^2}{\sigma_n^2 - 4\sigma^2} a_n \phi_n \sin 2\sigma t \sin 2px, \tag{3.1.36}$$

$$\rho = \Pi + \frac{\alpha^2 p^2}{8\sigma^2} [2\Psi\Psi'\Pi' + \Psi^2\Pi''] - \frac{\alpha p}{\sigma} \Pi' \Psi \cos \sigma t \cos px$$
$$+ \frac{\alpha^2 p^2}{8\sigma^2} \cos 2px \left\{ \Pi'' \Psi^2 - \left(\Pi'' \Psi^2 + 8\sigma^2 \sum_{n=1}^{\infty} \frac{a_n \Pi' \phi_n}{\sigma_n^2 - 4\sigma^2} \right) \cos 2\sigma t \right\} \tag{3.1.37}$$

and

$$\eta = \frac{\alpha p \Psi}{\sigma} \cos \sigma t \cos px + \frac{\alpha^2 p^2}{4\sigma^2} \cos 2px \left\{ \Psi\Psi' + \left[\Psi\Psi' + \sum_{n=1}^{\infty} \frac{a_n \sigma_n^2 \phi_n}{\sigma_n^2 - 4\sigma^2} \right] \cos 2\sigma t \right\}. \tag{3.1.38}$$

The distortion of the wave profile from sinusoidal at any height z, is given by the second-order terms. If

$$\sum_{n=1}^{\infty} \frac{a_n \sigma_n^2 \phi_n}{\sigma_n^2 - 4\sigma^2} \neq 0$$

at any given z then the wave profile there will never be completely flat (the nearest approach to a flat profile is at $t = \pi/2\sigma$). The mean density at any level is changed in the wave motion.

The general theory may easily be extended further to include higher-order effects, but the calculations made already allow the estimation of the distortion from sinusoidal of the wave profile in given density profiles. A higher-order expansion would lead to more accurate estimation of the wave profile,† and to an estimation of the effects of finite amplitude on the dispersion relation. We now leave the general theory and consider particular cases.

3.2. *Waves in a fluid of density* $\Pi(z) = 1-\mu z, \mu > 0$

In this case (3.1.18) becomes

$$\Psi_{,zz} - p^2(1-\mu/\sigma^2)\Psi = 0, \quad \Psi(0) = \Psi(\pi/r) = 0, \tag{3.2.1}$$

and solutions are

$$\Psi = \sin nrz, \quad \text{where} \quad n^2r^2 = p^2(\mu/\sigma^2 - 1). \tag{3.2.2}$$

(For real values of nr it is necessary that $\sigma^2 \leqslant \mu$, a consequence of the theorem of Groen 1948*b*. An arbitrary constant may be added to the expression for Ψ, but this may be absorbed in the parameter α.)

The expression for the frequency, σ, from (3.2.2) is

$$\sigma^2 = \frac{\mu p^2/\hat{W}^2}{(p^2/\hat{W}^2) + (n^2/\hat{H}^2)}, \tag{3.2.3}$$

since $r = \hat{W}/\hat{H}$. n is the number of half oscillations of Ψ in the vertical and p the number of half wavelengths in the horizontal between the vertical tank walls. The number pair (p, n) will be used to indicate the mode of oscillation which occurs in the experiments described below.

Returning to non-dimensional form, the particle displacement

$$\eta = A \sin nrz \cos px \cos \sigma t + \tfrac{1}{8}A^2 nr \sin 2nrz(1 + \cos 2\sigma t) \cos 2rx, \tag{3.2.4}$$

where $A = \alpha p/\sigma$ is a measure of the wave amplitude.

The wave profile is of immediate interest. Suppose for example that $n = 1$. Then at $t = 0$,

$$\eta = A \sin nrz(\cos px + \tfrac{1}{2}Ar \cos rz \cos 2px)$$

and so, if $0 < z < \pi/2r$, the wave profile is one in which the crest is narrower than the trough. It resembles in shape the surface standing wave profile. If, however, $\pi/2r < z < \pi/r$, the trough is narrower than the crest and the wave profile resembles an inverted surface standing wave (the analogy with interfacial waves is more direct as may be seen by comparing these results with those of §2). At time $t = \pi/2\sigma$, the surface is undisturbed to second order, $\eta = 0$ (unlike the interfacial waves, which showed a second harmonic at these times when one of the two fluids was shallow). These waves, with $n = 1$, have a vertical wavelength of twice the fluid depth. The wave profile for higher values of n may be similarly be examined.

† This is on the assumption, made throughout, that the series expansions, (3.1.8), (3.1.9), are convergent.

The expressions for the stream function, ψ, and density, ρ, of the fluid are

$$\psi = (A\sigma/p)\sin nrz \sin\sigma t \sin px$$

and

$$\rho = 1-\mu z+\mu A \sin nz\cos\sigma t\cos px-\tfrac{1}{8}A^2\mu nr\sin 2nrz\,(1+\cos 2\sigma t).$$

If the expansion is carried to third order, the fluid displacement is

$$\begin{aligned}\eta = {} & A\sin rnz\cos px\cos\sigma t+\tfrac{1}{8}A^2nr\sin 2nrz(1+\cos 2\sigma t)\cos 2px\\ & +\frac{n^2r^2A^3}{128}\Big\{\cos px\sin nrz(3\cos\sigma t-2\cos 3\sigma t)\\ & +\cos px\sin 3nrz\left[\frac{\sigma^2}{\mu-\sigma^2}\cos\sigma t-\frac{3(\mu-\sigma^2)}{10\mu-9\sigma^2}\cos 3\sigma t\right]\\ & +\cos 3px(3\cos\sigma t+\cos 3\sigma t)\,(5\sin 3nrz-7\sin nrz)\Big\}, \qquad (3.2.5)\end{aligned}$$

while the third-order correction to the dispersion relation is to make

$$\sigma = \sigma_0\left(1-\frac{n^2r^2A^2}{32}\right),$$

where $\sigma_0^2 = p^2\mu/(p^2+n^2r^2)$, the first-order solution. (The expressions for ψ and ρ are given in appendix 3.)

The effect of finite wave amplitude is thus to decrease the wave frequency, irrespective of fluid depth, in contrast to the findings in the case of surface and interfacial waves when critical depth to wavelength ratios exist, below which the frequency increases with wave amplitude.

It will be noticed that the coefficients which occur in (3.2.5) are finite, since $\sigma^2 < \mu$ for non-zero values of (n/p), and, if nrA is sufficiently small, there is some indication that the series is tending to converge. The parameter which must be small when we dimensionalize, is $\hat{A}\hat{l}$ where $\hat{A}$ is a wave amplitude measure and $\hat{l}$ is the vertical wave-number of the waves. The fluid displacement is zero at time $t = \pi/2\sigma$.

If the upper boundary of the fluid is free, then it may easily be shown that, if $\pi \gg \mu r^2$, the frequency of an internal mode of oscillation is given by

$$\sigma^2 = \frac{\mu p^2}{p^2+m^2r^2[1+2\mu r^2/\pi(m^2r^2+p^2)]}, \qquad (3.2.6)$$

where m is the largest positive integer less than y, a solution of

$$\tan\pi y = \frac{y\mu r^2}{r^2y^2+p^2}.$$

The effect of the free surface on the profile of the internal oscillation is negligible if, in dimensional units

$$\frac{\hat{\rho}_0(0)-\hat{\rho}_0(\hat{H})}{2\pi\hat{\rho}_0(0)}\frac{\hat{l}}{\hat{k}} \ll 1,$$

where $\hat{k}$ is the horizontal wave-number and $\hat{l}$ the vertical wave number. In the experiments this condition will be well satisfied.

3.3. *Waves in an unbounded fluid density of* $\Pi(z) = 1 - \Delta \tanh az$

The solutions of (3.1.18) corresponding to various modes of the system have been discussed in some detail elsewhere (Groen 1948*a*; Thorpe 1968). The solution for Ψ for the first mode is

$$\Psi = \operatorname{sech}^{p/a} az,$$

where

$$\sigma^2 = \frac{\Delta ap}{p+a}.$$

Substitution into (3.1.37) gives the equation for η correct to second order

$$\eta = A \operatorname{sech}^{p/a} az \cos px \cos \sigma t - \tfrac{1}{4} A^2 p \cos 2px \operatorname{sech}^{2p/a} az \tanh az \left(1 + \frac{3p}{3p+2a} \cos 2\sigma t\right),$$

where $A = \alpha p/\sigma$. (The solutions ϕ_n are exactly as found in the paper on progressive waves by Thorpe (1968, equation (3.3.19)). As in that paper, the solutions are not valid for very long waves, and do not therefore reduce to the form found for interfacial waves in deep water discussed in §2.) Solutions for higher modes may also be found.

3.4. *Experiments*: $\Pi(z) = 1 - \mu z, \mu > 0$

The experiments were made using the apparatus described in the experiments on interfacial standing waves in a two fluid system discussed in §2. The same apparatus was used to fill the tank as in that experiment. The tank was filled layer by layer, each of the same thickness (usually 1 cm) and each being denser than the preceding layer by a constant amount, the density variation being achieved by the addition of brine. A little gentian violet was added to every third layer to allow the motions of the lines of constant density to be followed. The density difference between each layer, measured by the salinometer calibrated for density, was usually 0·0005 g/c.c. The tank was filled until the fluid was level with the tops of the plungers, when there were about forty layers of graded density. The fluid was allowed to stand for a few hours before the experiments began to allow for diffusion; when the experiment was begun it was thought that the density gradient in the fluid differed only slightly from a constant value, a conclusion recently substantiated by the experiments of Mowbray (1967), and the situation therefore closely resembled that envisaged in §3.2 except that the upper surface of the fluid was free and not fixed horizontally.

The experiments were designed: (*a*) to examine the sorts of wave motion which may occur in a uniformly stratified fluid; (*b*) to examine the frequency of the various modes when the wave amplitude is small and to make a comparison with theoretical predictions; (*c*) to examine the wave profiles, particularly at finite amplitudes; (*d*) to find what, if any, effects occur when the wave amplitude becomes very large.

In all the experiments, the density difference between the top and bottom of the fluid was small compared with a mean density, and therefore to a first approximation the main body of the fluid should oscillate as if there were a fixed boundary at the free surface, as explained above. We therefore compare the

observations with the theoretical results for a fluid bounded above at the experimental free surface.

With plungers working in opposition, two different modes could be easily generated. The appearance of these is shown in figure 21 and 22, plate 8. The first corresponds to mode (2,1) and the second to (2,3). Higher modes were not

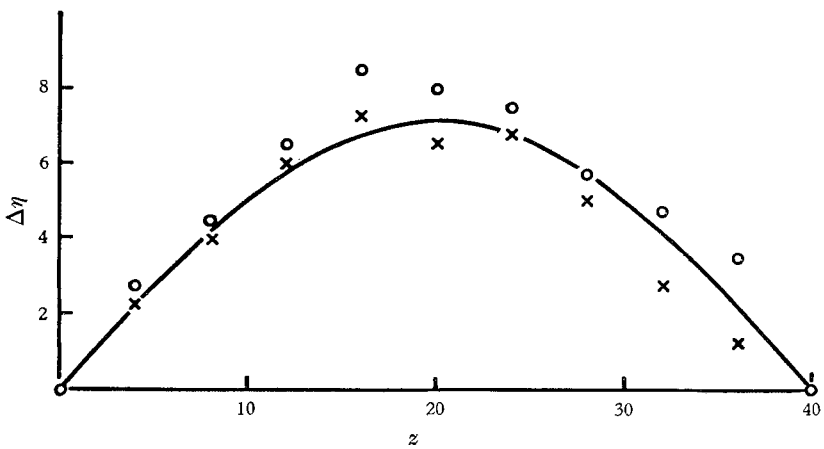

FIGURE 23. The variation of the total amplitude of particle displacements, $\Delta\eta$, with height above the bottom of the tank, z, measured in centimeters, from figure 21. The full line is a sine curve, proportional to sin $(\pi z/H)$.

Mode	Observed times of one oscillation (s)	Observed mean period (s)	Predicted period (s)	Difference between observation and prediction (%)
(2,1)	9·92, 9·91, 9·96, 9·87, 9·94, 9·905	9·92	9·84	0·81
(2,3)	14·99, 14·93, 14·86 14·9, 15·15, 15·07	14·98	14·92	0·40

TABLE 1. Comparison of predicted and observed standing wave frequencies. Observed times of one oscillation are deduced from timing 10 free oscillations. The predicted periods are based on (3.2.5)

examined. The (2,2) mode could not be generated with the plungers moving in opposition. The frequencies of these waves were found by timing about 10 free oscillations with a stop watch. The results are shown in table 1. The predictions are based on the estimated frequencies using (3.2.6) for the frequency of waves with a free upper surface. The comparison of theory and experiment is satisfactory. The effects of fluid viscosity on the frequency are considered later and found to be negligible.

With the plungers working in phase, the (1,1) mode could be excited. The frequency of waves in this mode was found from two sets of observations to be 0·514 rad/s as compared with the predicted 0·525 rad/s.

Measurements made from the wave profiles of the (2,1) mode indicate that the variation of particle displacement with height above the bottom of the tank is approximately sinusoidal (figure 23). The wave profile (η *vs* x) is not, however, well described by the predictions of the second-order theory, although the wave amplitude was such that second order effects should have been noticeable. It appears that the wave profiles at large amplitude were markedly distorted by two effects; (*a*) the presence of other modes of the system excited by the plunger motion, and (*b*) the presence of rays of internal waves of small wavelength propagating away from the bottom of the two plungers and generated as a result of the vertical fluid motion past the slight depressions in the tank walls at the bottoms of the plungers. These effects are discussed below. The effects were (accidentally) avoided in another experiment, one on progressive waves in a stratified fluid (Thorpe 1968). In this experiment internal waves of the first (vertical) mode in a fluid of constant density gradient were generated by a wave maker at one end of a long tank. The waves arriving at the other vertical end of the tank were reflected and standing waves resulted nearby. These are shown in figure 26, plate 10. Although no quantitative comparison with theory is possible, these waves are seen to have the predicted form.

Large-amplitude effects

As the amplitude of the plunger motion was increased, the maximum amplitude which might be obtained by the wave motion in any mode increased. No detailed investigation of this qualitative observation was made, since it was not possible to measure the vertical motion of the diffuse layers of dye accurately,† but in the (2,1) mode with a plunger total amplitude of 0·65 cm, the maximum total wave amplitude which could be generated was about 3·8 cm.

The damping of the free wave motion was not very great. In the mode (2,1) during the time of ten free oscillations measured as 99·2 s, the total wave amplitude was observed to decrease from about 3·5 cm to 2·5 cm, corresponding to a damping coefficient, q, of $3{\cdot}36 \times 10^{-3}\,\mathrm{s}^{-1}$ (where the amplitude at time t, $A(t) = A(0)\,e^{-qt}$). In appendix 4 we estimate the viscous dissipation of energy in the fluid. The damping coefficient found theoretically which corresponds to the conditions above, is $q = 5{\cdot}3 \times 10^{-3}\,\mathrm{s}^{-1}$, which is a little larger than that observed; the measurements of amplitude, however, are only approximate.

When the total plunger amplitude was increased to 1·1 cm, and the frequency set near that of free oscillation in the (2,1) mode (the plunger frequency was 0·628 rad/s^{-1}), the wave amplitude gradually increased during the first 10 oscillations and by the 15th oscillation some irregularity in the wave motion was observed. The shape of the wave profile during subsequent oscillations is shown in the sequence of photographs figure 24, plate 9. Serious irregularities dominated the wave profile, although there remained the dominating primary oscillation of the plunger frequency. The photographs shown were taken in every other cycle when the upward fluid displacement at the centre of the tank reached its maxi-

† Other methods of measurement might have been used, but the main focus of attention was on free wave oscillation and the effects which occurred at large forced oscillation.

mum value. Mixing and overturning were seen to occur in the regions where the irregularities were greatest (figure 24*f*, *g*, *h*) although after the motion of the plungers was stopped, the plungers having made a total of 33 oscillations, the motion of the fluid died out and the bands of dye remained still clearly defined, if a little more diffuse. If the plunger motion was arrested as soon as any irregularity was observed, then the sequence of breaking continued to manifest itself in just the same way as when the plunger motions were continued. It is probable that some of the irregularities observed occur as the result of waves which do not satisfy exactly the frequency equation. Quite a large response may be obtained when the plunger frequency is a few per cent away from the natural wave frequency, and it seemed possible that the irregularities in the wave profile were

Horizontal modal number, p	Vertical modal number, n = 1	2	3	4	5
1	0·525	0·344	0·246	0·190	0·154
2	0·638	0·525	0·421	0·344	0·288
3	0·672	0·603	0·525	0·452	0·392
4	0·683	0·638	0·583	0·525	0·469
5	0·690	0·660	0·618	0·571	0·525

TABLE 2. The theoretical angular frequency, σ, in rad/s for different model numbers (p, n) possible in the experiments

associated with the incidental generation of modes with frequency near the plunger frequency in the experiment. Table 2 shows the frequency of various modes which correspond to the experimental conditions (density gradient 5×10^{-4} g/c.c./cm, fluid depth 40 cm, width 35·5 cm). The frequency of the plungers, during the period in which the sequence of photographs (figure 24) was taken, was 0·628 rad/s^{-1}, slightly less than the natural calculated frequency of the waves in the (2,1) mode at small amplitude. This frequence is of course the same as that of the (4, 2) mode, but we expect from earlier observations that only waves with an odd vertical and an even horizontal modal number will be excited by plungers working in opposition, and in fact, the (4, 2) mode was not observed. A brief examination of table 2 suggests that the most probable mode which might be generated at the same time as the (2, 1) mode by plunger oscillation slightly less than 0·638 rad/s^{-1}, is the (4, 3) mode. Examination of the photographs strongly suggests the existence of this wave mode (see, for example, figure 24*h*), and the irregularities seen in the photographs are partly the result of the presence of two modes, the (2, 1) and the (4, 3).

The small-scale irregularities appear to originate from the bottom of the plungers and have a form very similar to that associated with rays of internal waves (see, for another example, Thorpe 1968). In an undisturbed fluid a ray of internal waves of frequency σ in fluid of constant stability frequency N would propagate at an angle $\alpha = \sin^{-1}(\sigma/N)$ to the horizontal, although the propagation path in the presence of standing waves would be disturbed, the wave belonging

to the rays being convected with the standing wave motion (for further discussion see Bretherton 1966). Using the facts that $\sigma = Nk(k^2+n^2)^{-\frac{1}{2}}$ (dimensional variables) and for the (2, 1) mode the horizontal and vertical wave-numbers (k, n) of the primary standing wave are $(2\pi/W, 2\pi/2H)$ for the tank of width W and height H, it is easily shown that $\tan\alpha = 2H/W$. The mean paths of the internal wave rays are therefore as shown in figure 25. It is thought that the small scale irregularities and regions of local overturning are the result of the distortion of the internal wave rays by the standing wave motion. It seem unlikely that instability might be caused by local shears generated in the wave motion, as the estimated minimum local Richardson number was about 60 and the motion should therefore be very stable.

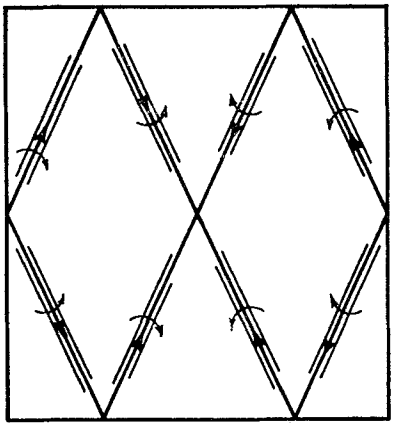

FIGURE 25. The paths of internal wave rays originating from the bottom of the plungers. The curved arrows indicate the direction of the phase velocity, full arrows the group velocity. Cusped reflexion at the top and bottom boundaries, where diffusion destroys the density gradient, is expected although not shown in the sketch.

More exhaustive experiments on standing internal waves in a fluid of constant density gradient have been made by Dr K.–H. Keunecke of the Ozeanographische Forschungsanstalt der Bundeswehr, Kiel, and it is hoped that these may be published shortly. Full agreement with the present results has been found.

This investigation of standing internal waves is part of a general study of breaking internal waves, and was made in the Department of Applied Mathematics and Theoretical Physics at Cambridge. The apparatus was made at the University Engineering Laboratories and I am grateful for the advice of Mr Barker during the construction, and for the use of the heat sealing apparatus at the Low Temperature Research Station in Cambridge used in making the polythene bags.

Appendix 1

For $\rho_2 - \rho_1$ not much less than ρ_2, and for a two fluid model with a fixed upper surface, we find the interfacial wave profile

$$\zeta = a\sin\sigma t\cos kx + a^2k(z_1 + z_2\cos 2\sigma t), \qquad \text{(A 1.1)}$$

where $$z_1 = \frac{T_1 T_2}{8(\rho_1 T_2 + \rho_2 T_1)}\left[\rho_2 - \rho_1 + \frac{1}{T_1^2 T_2^2}(\rho_2 T_1^2 - \rho_1 T_2^2)\right]$$

and $$z_2 = \frac{1}{8(\rho_1 T_1 + \rho_2 T_2)}\left[\rho_1 - \rho_2 + \frac{3}{T_1^2 T_2^2}(\rho_1 T_2^2 - \rho_2 T_1^2)\right]. \qquad \text{(A 1.2)}$$

If $\rho_1 = 0$, this reduces to the solution for surface standing waves of Tadjbakesh & Keller.

For two fluids with a free upper surface, the elevation of the interface, ζ, is defined as in (A 1.1) but where

$$z_1 = \frac{p}{8(\rho_2 - \rho_1)}\left[2(\rho_2 - \rho_1) + \frac{\rho_2}{\sinh^2 kh_2} - \frac{\rho_1(1-p^2)}{r^2 \sinh^2 kh_1}\right],$$

$$z_2 = -\frac{p}{8(\rho_2 - \rho_1)}\left\{2(\rho_2 - \rho_1) - \frac{\rho_2}{\sinh^2 kh_2} + \frac{\rho_1(1-p^2)}{r^2 \sinh^2 kh_1}\right.$$

$$\left. - 2E\left[\rho_1(1 - 2pT_1) + \frac{\rho_2}{S_2}(T_1 - 2p)\right] - \frac{2}{T_2}[2p_2 B + A(\rho_2 + \rho_1 S_1 S_2)]\right], \qquad \text{(A 1.3)}$$

where $$p = \sigma^2/gk, \quad r = 1 - p/T_1, \quad A = 3p(1-p^2)(1-T_1^2)/T_1^2 r^2,$$

$$B = [T_1 + T_2 - p(1 + T_1 T_2)]/rT_1 T_2,$$

$$C = 2(\rho_2 - \rho_1)\left(\frac{1}{T_2} - p\right) + p\left[\frac{\rho_2}{\sinh^2 kh_2} - \frac{\rho_1(1-p^2)}{r^2 \sinh^2 kh_1}\right],$$

$$E = \frac{1}{R}\left\{S_2\left[C + 2B\left(\frac{2pp_2}{S_2} - \rho_2 + \rho_1\right)\right] + A[2p(\rho_1 S_1 S_2 + \rho_2) - S_2(\rho_2 - \rho_1)]\right.,$$

$$R = 4p^2(\rho_1 S_1 S_2 + \rho_2) - 2p\rho_2(S_1 + S_2) + (\rho_2 - \rho_1) S_1 S_2,$$

and $$S_i = \tanh 2kh_i.$$

The corresponding equation of the free surface is

$$\eta = \alpha \sin \sigma t \cos kx + \alpha^2 k(N_1 + N_2 \cos 2\sigma t) \cos 2kx,$$

where

$$\alpha = -\frac{ap}{r \sinh kh_1}, \quad N_1 = \frac{1+p^2}{8p} \quad \text{and} \quad N_2 = -\frac{1}{8p}(3p^2 - 1 + 2Er^2 \sinh^2 kh_1).$$

These results reduce to those of Tadjbakesh & Keller when the appropriate approximations are made, and the equation of the interface reduces to Hunt's (1961) solution when kh_1, kh_2, are large.

If the internal wave mode is excited and $(\rho_2 - \rho_1)/\rho_2$ is small, the surface wave disturbance tends to zero and the solution for the interface, ζ, tends to the solution (A 1.2) for a fixed boundary.

If the fluid below the interface is deep, so that $kh_2 \gg 1$ and $T_2 = 1$, it is easy to find the effect of non-homogenity of density on the dispersion relation of the surface waves. For the surface mode, it is found that

$$\sigma^2 = gk\left[1 - \frac{\alpha^2 k^2}{4}\left(\frac{\rho_1(1+T_1) + (\rho_2 - \rho_1)(1 - T_1)\, e^{-2kh_1}}{2(\rho_1 T_1 + \rho_2) - \rho_2(1 + T_1)}\right)\right],$$

correct to third order, where α is the first-order wave amplitude. This expression reduces to $\sigma^2 = gk[1-\alpha^2k^2/4]$ if $\rho_2 = \rho_1$, the result shown by Penney & Price for deep water standing waves. If $\rho_2 = \rho_1(1+\mu)$, and $\mu \ll 1$, we find

$$\sigma^2 = gk\left\{1-\frac{\alpha^2k^2}{4}\left[1-\frac{\mu(1-T_1)}{1+T_1}(1-e^{-2kh_1})+O(\mu^2)\right]\right\}$$

and the effect of a small density difference is to increase the surface wave frequency.

Appendix 2

1. The effect of a non-sharp interface

In order to estimate the change in frequency of interfacial waves due to some mixing at the interface, a three-layer model was considered in which the densities, ρ_1 and ρ_2, of the upper and lower fluids were constant, whilst the density of the intermediate region of thickness $2d$ was $\rho e^{-\mu z}$ (z being taken vertically upwards), and equal to ρ_1 at $z = d$, and ρ_2 at $z = -d$. For simplicity it was assumed that the upper fluid was deep and the lower of depth h_2. This system has infinitely many modes of vibration, but it is possible to select the primary mode which reduces to the mode in a two fluid system when the thickness of the intermediate layer tends to zero. This model will not accurately resemble the experimental situations, but should indicate the effect of the intermediate layer fairly well.

If the density difference between the upper and lower fluids is small, and if kd is small, where k is the wave-number of the standing oscillation, then the frequency, σ, is given by

$$\begin{aligned}\sigma^2 &= \frac{gk\tanh kh_2(\rho_2-\rho_1)}{\rho_1(1+\tanh kh_2)}[1-\tfrac{2}{3}kd(2\tanh kh_2-1)]\\ &= \sigma_0^2[1-\tfrac{2}{3}kd(2\tanh kh_2-1)] \qquad \text{(A 2.1)}\end{aligned}$$

approximately, where σ_0 is the frequency of interfacial waves in the two fluid system.

Hence the effect of the transition layer is to decrease the wave frequency if both fluids are deep, and to increase the frequency if the lower fluid is sufficiently shallow ($h_2 < (k\tanh\frac{1}{2})^{-1}$).

A decrease in frequency with increase in thickness of the transition layer, was observed in the experiments in deep water. A transition layer of thickness about 2 cm (based on a calculation using this model) would be necessary to produce the 6 % variation in observed frequencies from those calculated on the basis of a two fluid model.

2. The effect of viscosity

(a) At the fluid interface

Harrison (1908) showed that the effect of viscosity on waves at the interface between two deep fluids is to decrease the frequency, σ, from the inviscid theoretical frequency σ_0, by an amount

$$\Delta\sigma = \frac{k}{2}\left(\frac{\sigma_0\nu}{2}\right)^{\frac{1}{2}} \qquad \text{(A 2.2)}$$

if $\rho_2-\rho_1 \ll \rho_1$.

If we take $\sigma_0 = 0{\cdot}6$ rad/s, $k = 0{\cdot}177$ cm^{-1}, and the kinematic viscosity (taken at the same value in each fluid), ν, $= 0{\cdot}01$ cm^2 s^{-1}, to represent typical scales used in the experiments, then the effect of viscosity is to decrease the frequency by about $0{\cdot}8\,\%$. This is based on the assumption that no mixing occurs and that the interface is sharp. A thin transition region may well decrease this estimate substantially.

The effect of viscosity is also to decrease the amplitude, $A(t)$, of the wave, so that

$$A(t) = A(0)\,e^{-qt}, \quad \text{where} \quad q = \Delta\sigma. \tag{A 2.3}$$

The damping coefficient, q, is increased when the depth of the upper fluid is decreased.

(*b*) *Viscosity at the boundaries*

Using the theory given in Lamb (1932, §§329, 345), it is easy to compute the rate of energy dissipation from the wave motion by viscosity at the walls of the tank.

If W is the width and B the breadth of the tank, and if the upper fluid is deep and the lower of depth h_2, then the rate of loss of energy in the tank due to viscosity at the walls and bottom is

$$\frac{A^2}{2}\left(\frac{\sigma\nu}{2}\right)^{\frac{1}{2}}\left[g(\rho_2-\rho_1)(B+W)+\frac{\sigma^2\rho_2 B(W-2h_2)}{2\sinh^2 kh_2}\right] \tag{A 2.4}$$

when the wave amplitude is A and the coefficient of viscosity ν, is equal in the two fluids. Hence the effect of a shallow lower layer is to increase the rate of loss of energy in the wave motions.

Now the energy density per unit horizontal area of the interfacial standing wave motion is

$$\tfrac{1}{4}A^2 g(\rho_2-\rho_1). \tag{A 2.5}$$

Hence if E^* is the total energy of the standing wave motion in the tank, when both fluids are deep and the viscous effects at the interface are neglected, by combining (A 2.4), (A 2.5) we have

$$E^*(t) = E^*(0)\exp\left\{-(2\sigma\nu)^{\frac{1}{2}}\frac{(B+W)}{BW}t\right\}.$$

The equation including the effect of viscosity at the interface is

$$E^*(t) = E^*(0)\exp\{-(\tfrac{1}{2}\sigma_0\nu)[2(B+W)/BW+k]t\} \tag{A 2.6}$$

from (A 2.3).

For the wave with modal number n, $k = n\pi/w$, and the ratio of dissipation at the walls to that at the (sharp) interface is $2(B+W)/n\pi B$. (The corresponding damping coefficient is

$$q = [(B+W)/BW+k/2](\sigma\nu/2)^{\frac{1}{2}},$$

and if $\sigma = 0{\cdot}9$ rad s^{-1}, $\nu = 0{\cdot}01$ cm^2 s^{-1}, $B = 20{\cdot}3$ cm, $W = 35{\cdot}5$ cm, $k = 0{\cdot}177$ cm^{-1}, then $q = 1{\cdot}2\times10^{-2}$ s^{-1}. This agrees well with the estimate from observations mentioned above.) Equation (A 2.6) seems at first sight to lead to a contradiction with the observed response curves, figure 12. The rate of dissipation of energy is

$$[2(B+W)/BW+k](\sigma_0\nu/2)^{\frac{1}{2}}E^*(t),$$

or

$$[2(B+W)/BW+k/2]A^2BW(\rho_1+\rho_2)(\sigma_0^5\nu/2)^{\frac{1}{2}}/4k, \tag{A 2.7}$$

since $\quad E^*(t) = \tfrac{1}{4}A^2g(\rho_2-\rho_1)BW \quad$ and $\quad \sigma_0^2 = gk(\rho_2-\rho_1)/(\rho_1+\rho_2)$

and thus the loss of energy per cycle increases with frequency (or density difference). We have observed that the response curves figure 12, show an increase in the resonant amplitude with frequency for fixed plunger amplitude. This apparent contradiction can only be resolved if the plungers can put more energy into the wave motion at one frequency than they can at another lower frequency (or if the waves receive more energy from the plungers as the density difference between the fluids increases).

The rate of working of a plunger is $\int_s pv\,ds$, where p is the fluid pressure at the plunger, v is the plunger velocity, and the integral is taken over the area of the plunger, S. If we assume that exactly at resonance (that is when the plunger frequency is exactly the same as the natural frequency of the wave at the amplitude at which it is oscillating) at the crest of a response curve, there is a phase difference, ϵ, between the wave motion and the plunger motion, then the application of first-order wave theory leads to the result that the mean rate of working of one plunger on the fluid is approximately

$$a\sigma_0^3\rho_1 AB\sin\epsilon/2k^2.$$

Here we assume that only the upper fluid of density ρ_1 is in contact with the plunger, and that the plunger amplitude is a. Equating the energy input rate from two plungers to the rate of viscous dissipation at the boundaries, when both fluids are deep and the density difference between the fluids is small, we find

$$A = a(2\sigma/\nu k^2)^{\frac{1}{2}}\sin\epsilon B/(W+B). \tag{A 2.8}$$

If we substitute the values taken by the quantities k, B and W, in the experiment and take $\nu = 0{\cdot}01$ cm^2 sec^{-1}, we obtain

$$A = 50{\cdot}8a\sigma^{\frac{1}{2}}\sin\epsilon, \tag{A 2.9}$$

where A, a and σ are measured in c.g.s. units.

A plot of the values of the resonant wave amplitudes, A, against plunger amplitude, a, at fixed frequency, $\sigma = 0{\cdot}628$ s^{-1} (from figure 8) is approximately a straight line of slope 3·33, giving a value of $\sin\epsilon = 0{\cdot}0827$, and confirming the predicted relation between A and a. Moreover, a plot of A against $\sigma^{\frac{1}{2}}$ for fixed plunger amplitude, $a = 0{\cdot}175$ cm, values being taken from figure 12, lies approximately on a straight line of slope 0·148. This confirms the prediction of (A 2·9) and leads to another estimate of $\sin\epsilon = 0{\cdot}0833$, in remarkably good agreement with the first. The predicted phase angle, ϵ, between the plungers and the wave motion is thus about 4° 46′, which would not be detected in the experiments.

Appendix 3

For a linear density gradient, to third order

$$\psi = \frac{A\sigma}{r}\sin nz\sin\sigma t\sin rx + \frac{A^3\sigma\mu^2}{128r}\left[\frac{\sin 3nz\sin\sigma t}{\mu-\sigma^2} + \frac{\sin 3nz\sin 3\sigma t}{10\mu-9\sigma^2} - \frac{\sin nz\sin 3\sigma t}{\mu}\right]\sin rx,$$

and

$$\rho = 1-\mu z+\mu A \sin nz\cos\sigma t\cos rx-\tfrac{1}{8}A^2\mu n\sin 2nz(1+\cos 2\sigma t)$$
$$+\frac{A^3\sigma^2\mu n^2}{128r^2}\left[\frac{r^2+9n^2}{\mu-\sigma^2}\sin 3nz\cos\sigma t+\frac{3(r^2+9n^2)}{10\mu-9\sigma^2}\sin 3nz\cos 3\sigma t\right.$$
$$\left.-\frac{3(r^2+n^2)}{\mu}\sin nz\cos 3\sigma t\right]\cos rx.$$

Appendix 4. Viscous effects, continuous density

1. Damping due to viscosity in the body of the fluid

If viscous terms are included in the linearized vorticity equation, dropping the symbol (^) but retaining dimensional quantities, we obtain

$$\rho_0(0)\frac{\partial}{\partial t}\nabla^2\psi = g\frac{\partial\rho}{\partial x}+\nu\rho_0(0)\nabla^2(\nabla^2\psi), \tag{A 4.1}$$

where ν is the kinematic viscosity, which we suppose to be constant. The linearised equation of continuity is

$$\frac{\partial\rho}{\partial t}-\frac{\partial\psi}{\partial x}\frac{\partial\rho_0}{\partial z}=0. \tag{A 4.2}$$

The equation which results from the elimination of ρ from (A 4.1) and (A 4.2), and the substitution $\rho_0=\rho_0(0)(1-\mu z)$ is

$$\frac{\partial^2}{\partial t^2}\nabla^2\psi+\mu g\frac{\partial^2\psi}{\partial x^2}=\nu\nabla^2\left(\nabla^2\frac{\partial\psi}{\partial t}\right). \tag{A 4.3}$$

A solution is

$$\psi=\alpha\sin\frac{n\pi z}{H}\sin\frac{p\pi x}{W}e^{st}$$

(where H, W are the fluid height and width respectively), if

$$s^2\left(\frac{n^2}{H^2}+\frac{p^2}{W^2}\right)-\frac{\mu g p^2}{W^2}=\nu s\left(\frac{n^2}{H^2}+\frac{p^2}{W^2}\right)\pi^2. \tag{A 4.4}$$

(This does not satisfy the no-slip conditions at the walls; viscous damping at the walls is considered below.)

Hence $$s=i\sigma_0(1+\epsilon),$$

where $$\sigma_0=\left[\mu g\Big/\left(1+\frac{n^2W^2}{p^2H^2}\right)\right]^{\frac{1}{2}},$$

the frequency of inviscid waves, and

$$\epsilon=\frac{\nu\pi^2}{2\sigma_0}\left(\frac{n^2}{H^2}+\frac{p^2}{W^2}\right)\left[i+\frac{\nu\pi^2}{4\sigma_0}\left(\frac{n^2}{H^2}+\frac{p^2}{W^2}\right)\right]$$

if $$\frac{\nu\pi^2}{\sigma_0}\left(\frac{n^2}{H^2}+\frac{p^2}{W^2}\right)\ll 1.$$

The effect of viscosity is to introduce a dissipation coefficient

$$q_0 = \frac{\nu}{2}\pi^2\left(\frac{n^2}{H^2}+\frac{p^2}{W^2}\right) \tag{A 4.5}$$

and to increase the frequency, σ_0, by $(\nu^2\pi^2/8\sigma_0)(n^2/H^2+p^2/W^2)$, a negligible amount in the experiments.

2. Damping due to viscosity at the boundaries of the fluid

Using the method (Lamb 1932, §§329, 345) discussed by Schooley & Stewart (1963), the total mean rate of loss of energy due to viscosity at the fluid boundaries in the experiment is

$$-\frac{dE}{dt} = A^2\sigma^2\rho_0(\tfrac{1}{2}\sigma\nu)^{\frac{1}{2}}(\tfrac{1}{4}WHD)\left[\frac{1}{D}+\frac{2}{W}+\left(\frac{nW}{pH}\right)^2\left(\frac{1}{D}+\frac{1}{H}\right)\right], \tag{A 4.6}$$

where A is the wave amplitude, σ the frequency and H, W and D the fluid depth, width and breadth respectively.

The energy of standing internal waves in the tank is

$$E = \tfrac{1}{8}\rho_0 DHWA^2\sigma^2[1+(nW/pH)^2]$$

to second order, and so

$$\frac{1}{E}\frac{dE}{dt} = -\frac{(2\sigma\nu)^{\frac{1}{2}}}{1+(nw/pH)^2}\left[\frac{1}{D}+\frac{2}{W}+\left(\frac{nW}{pH}\right)^2\left(\frac{1}{D}+\frac{1}{H}\right)\right].$$

The energy is proportional to the square of the wave amplitude and so

$$A(t) = A(0)\exp(-q_1 t),$$

where the dissipation coefficient

$$q_1 = \left\{(\tfrac{1}{2}\sigma\nu)^{\frac{1}{2}}\left[\frac{1}{D}+\frac{2}{W}+\left(\frac{nW}{pH}\right)^2\left(\frac{1}{D}+\frac{1}{H}\right)\right]\right\}\Big/\left[1+\left(\frac{nW}{pH}\right)^2\right]. \tag{A 4.7}$$

In the experiments $H = 40$ cm, $W = 35{\cdot}5$ cm and $D = 20{\cdot}3$ cm, and q_1 is much greater than q_0, (A 4.5).

REFERENCES

Ayrton, H. 1908 *Proc. Roy. Soc.* A **80**, 252.

Ayrton, H. 1926 *Proc. Roy. Soc.* A **113**, 44.

Bretherton, F. P. 1966 *Quart. J. R. Met. Soc.* **92**, 466.

Carstens, T. 1964 Doctoral Dissertation, University of California.

Concus, P. 1962 *J. Fluid Mech.* **14**, 568.

Concus, P. 1964 *J. Fluid Mech.* **19**, 264.

Daly, B. J. 1967 *Phys. Fluids*, **10**, 297.

Fultz, D. 1962 *J. Fluid Mech.* **13**, 193.

Groen, P. 1948*a* *Kon Ned. Met. Inst., Med. en Verhand. Serie* B, **2**, 11.

Groen, R. 1948*b* *Physica*, **14**, 294.

Harrison, W. J. 1908 *Proc. Lond. Math. Soc.* (2), **6**, 396.

Hunt, J. N. 1961 *La Houille Blanche*, **4**, 515.

LAMB, H. 1932 *Hydrodynamics*, sixth ed. Cambridge University Press.
LIN, J. D. & HOWARD, L. N. 1960 *M.I.T. Hydrodyn Lab. Rept.* 44.
MARCOU, C. 1965 *C. r. hebd., Séanc. Acad. Sci., Paris*, Gp. 2, 260, nos. 2 and 3.
MORTIMER, C. H. 1952 *Phil. Trans.* B **236**, 355.
MOWBRAY, D. E. 1967 *J. Fluid Mech.* **27**, 593.
PENNEY, W. G. & PRICE, A. T. 1952 *Phil. Trans.* A **244**, 254.
PETTERSSON, O. 1909 *Publ. de Circonstances, Copenhagen*, p. 47.
PHILLIPS, O. M. 1966 *Dynamics of the Upper Ocean*. Cambridge University Press.
RAYLEIGH, LORD, 1896 *The Theory of Sound*, vol. 2. New York: Dover Publications.
ROSENHEAD, L. 1963 *Laminar Boundary Layers*. Oxford: Clarendon Press.
SCHMIDT, W. 1908 *Sber. Akad. Wiss. Wien, Math. Nat. Classe.* 117, ABTH 2A.
SCHOOLEY, A. H. & STEWART, R. W. 1963 *J. Fluid Mech.* **15**, 83.
SEKERZH-ZENKOVICH, YA. I. 1951 *Izv. Akad. Nauk. SSSR., Ser. Geofiz.* **5**, 68.
SEKERZH-ZENKOVICH, YA. I. 1961 *Trudy Morsk. Gidrofiz. Inst.* **23**, 1 (also *Dokl. Acad. Nauk. SSSR* **136**, 1).
STEARN, A. E., IRISH, E. M. & EYRING, H. 1940 *J. Phys. Chem.* **44**, 981.
STOKES, G. G. 1847 *Camb. Phil. Trans.* **8**, 441 (also Papers, Vol. 1).
TADJBAKHSH, I. & KELLER, J. B. 1960 *J. Fluid Mech.* **8**, 442.
TAYLOR, G. I. 1953 *Proc. Roy. Soc.* A **218**, 44.
THORPE, S. A. 1966 Ph.D. Thesis *Internal Gravity Waves*. University of Cambridge.
THORPE, S. A. 1968 In preparation.
WEDDERBURN, E. M. 1909 *Trans. Roy. Soc. Edinb.* **29**, 602.
WEDDERBURN, E. M. & WILLIAMS, A. M. 1911 *Phil. Trans. Edinb.* **47**, 619.
YIH, C-S. 1960 *J. Fluid Mech.* **8**, 481.

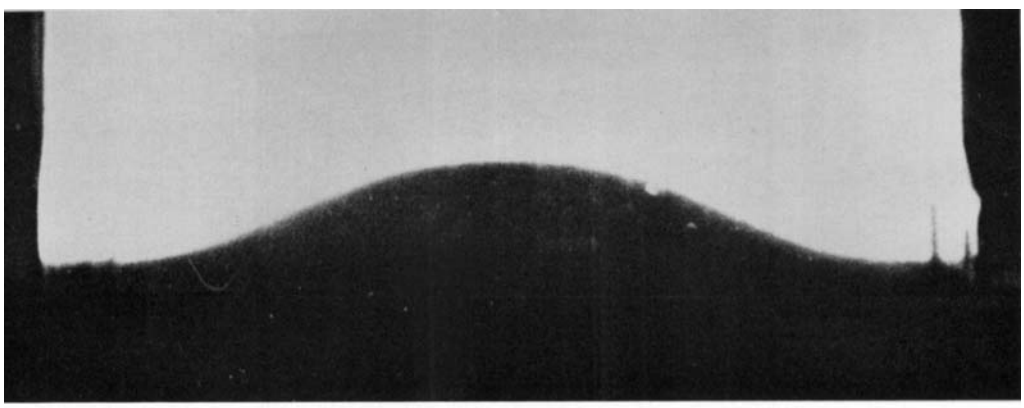

(*a*)

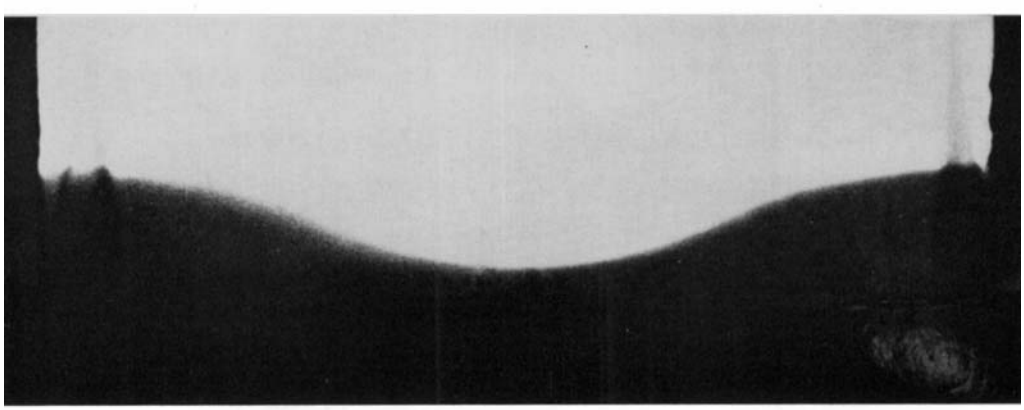

(*b*)

FIGURE 2. Interfacial waves between deep fluids. Mode $n = 2$. $h_1 = 25{\cdot}5$ cm. $h_2 = 19{\cdot}0$ cm. $\rho_2 - \rho_1 = 9{\cdot}0 \times 10^{-3}$ g/c.c., (*a*) maximum upward displacement; (*b*) maximum downward displacement.

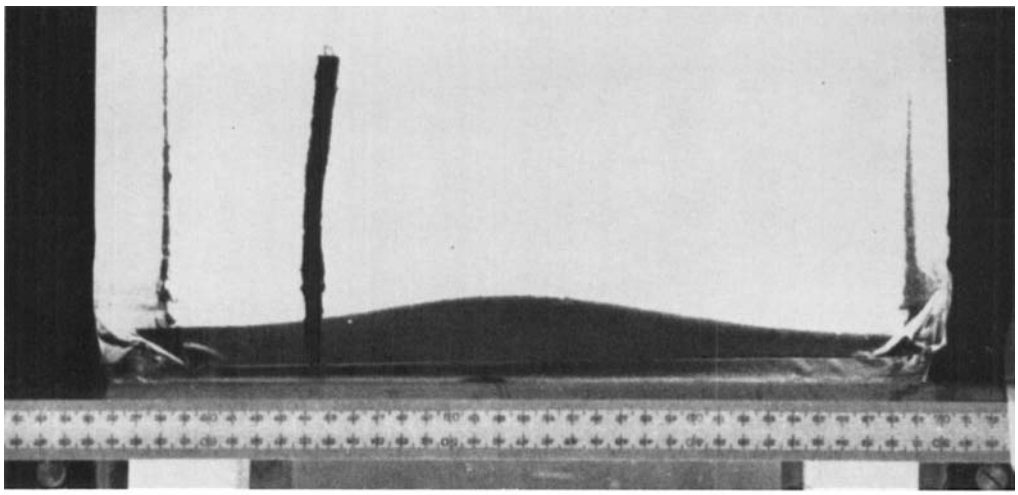

(*a*)

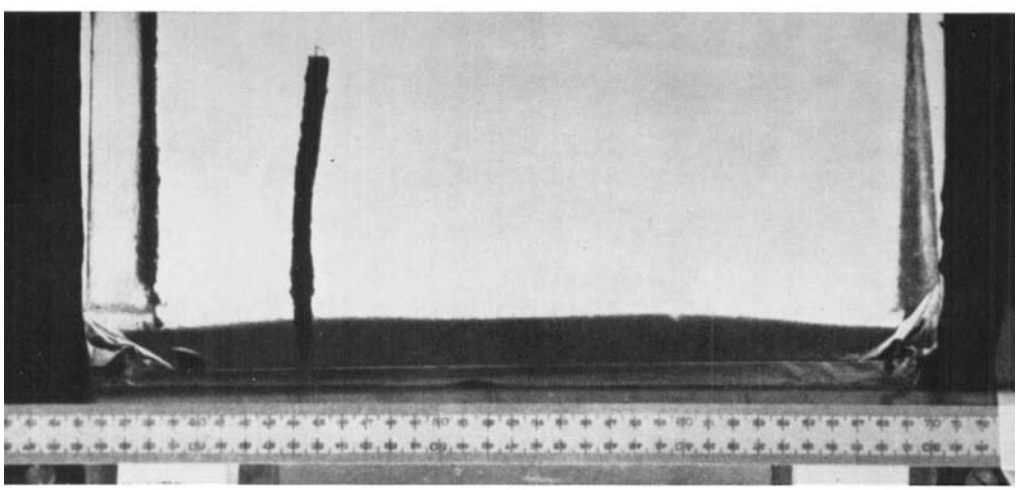

(*b*)

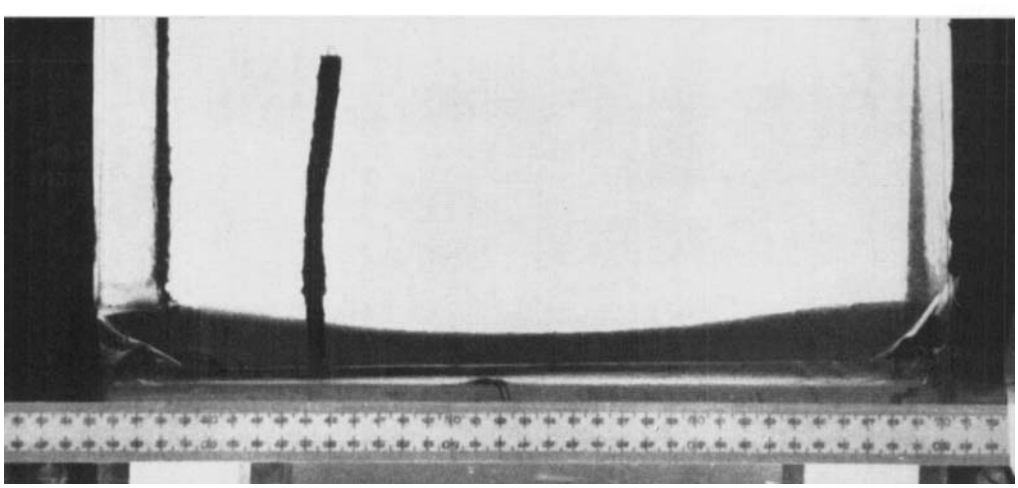

(*c*)

FIGURE 4. Interfacial waves in shallow lower fluid. $n = 2$, $h_1 = 27{\cdot}5$ cm, $h_2 = 2{\cdot}7$ cm, $\rho_2 - \rho_1 = 19{\cdot}8 \times 10^{-3}$ g/c.c. Wrinkles may be seen in the polythene in the corners of the tank, (*a*) maximum upward displacement; (*b*) minimum displacement; (*c*) maximum downward displacement.

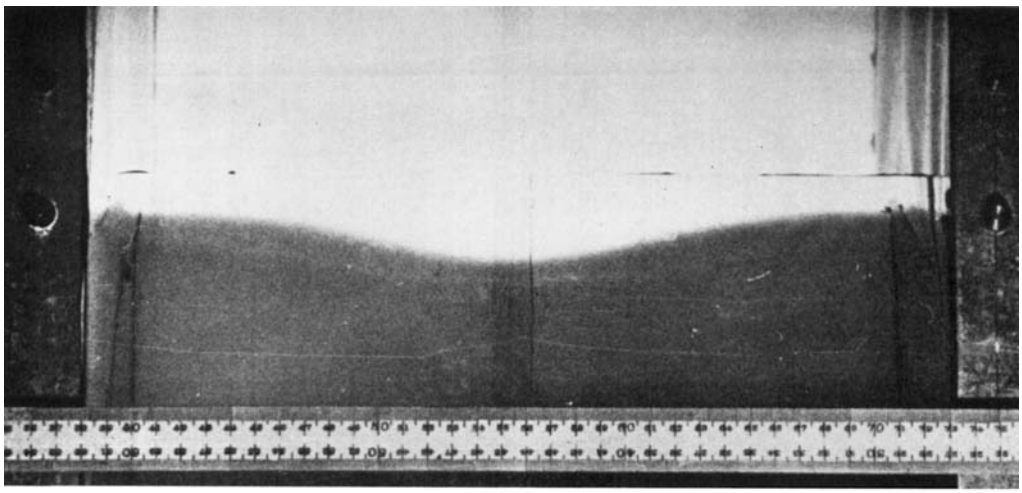

(*a*)

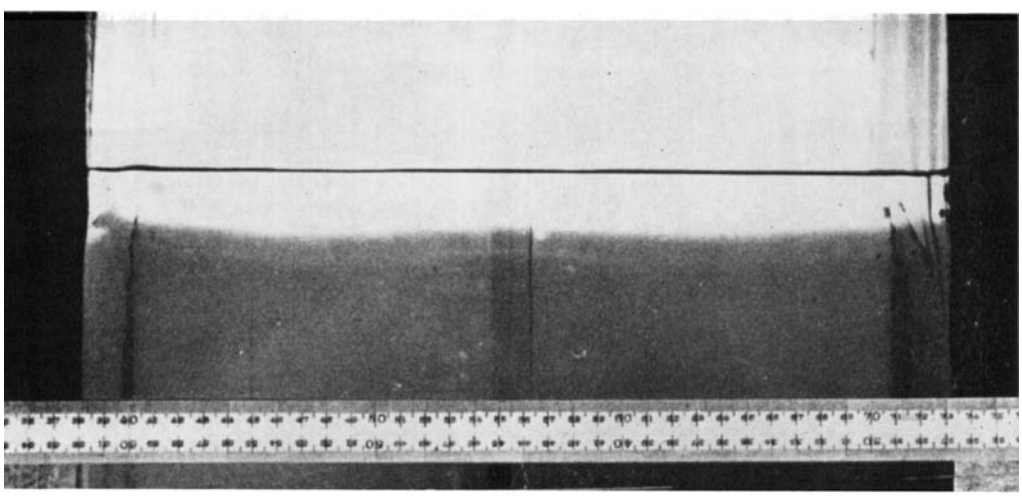

(*b*)

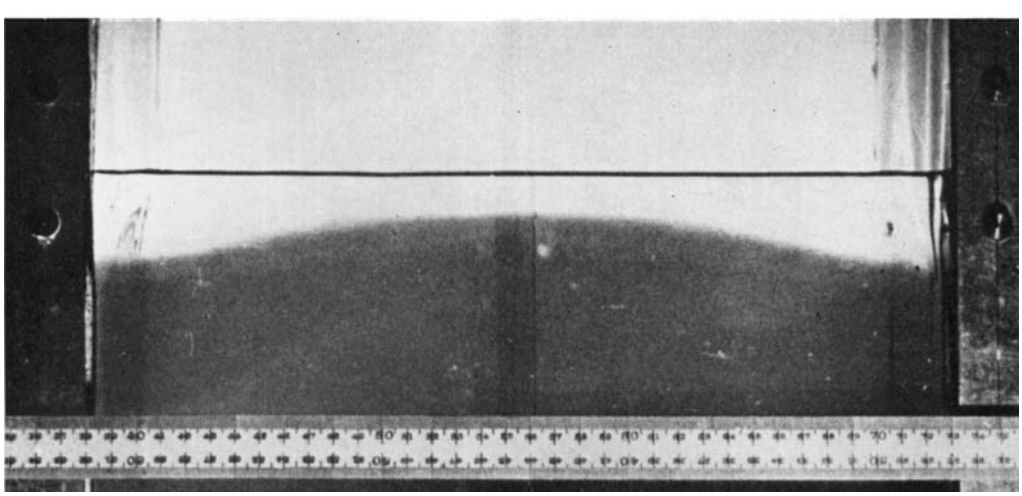

(*c*)

FIGURE 6. Interfacial waves in shallow upper fluid. $n = 2$, $h_1 = 2{\cdot}7$ cm, $h_2 = 23{\cdot}0$ cm, $\rho_2 - \rho_1 = 15{\cdot}5 \times 10^{-3}$ g/c.c., (*a*) maximum downward displacement; (*b*) minimum displacement; (*c*) maximum upward displacement.

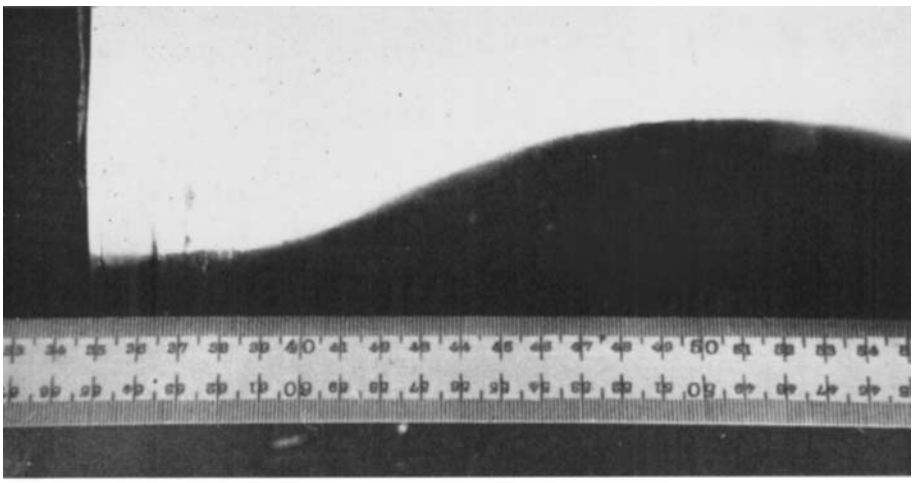

(*a*)

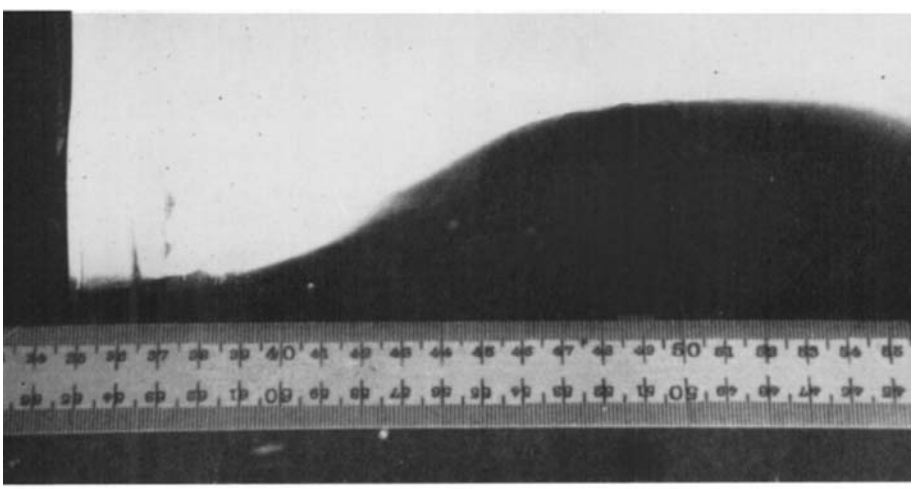

(*b*)

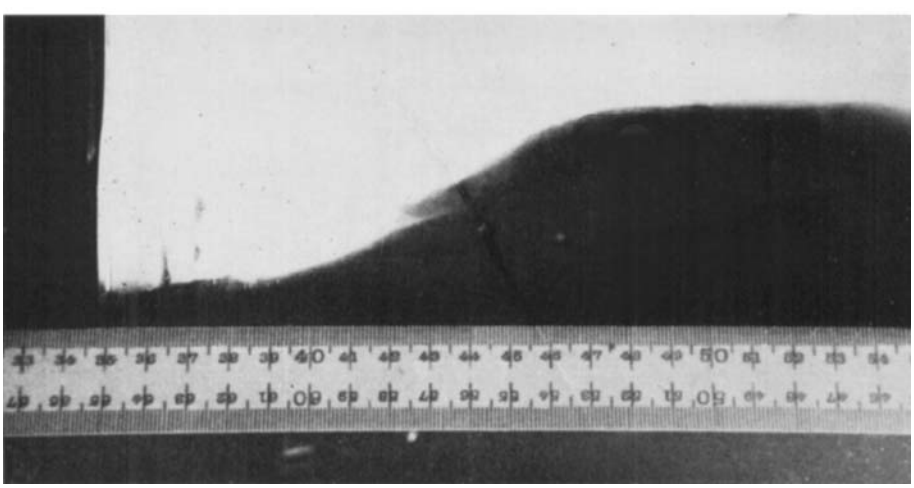

(*c*)

For legend see plate 5.

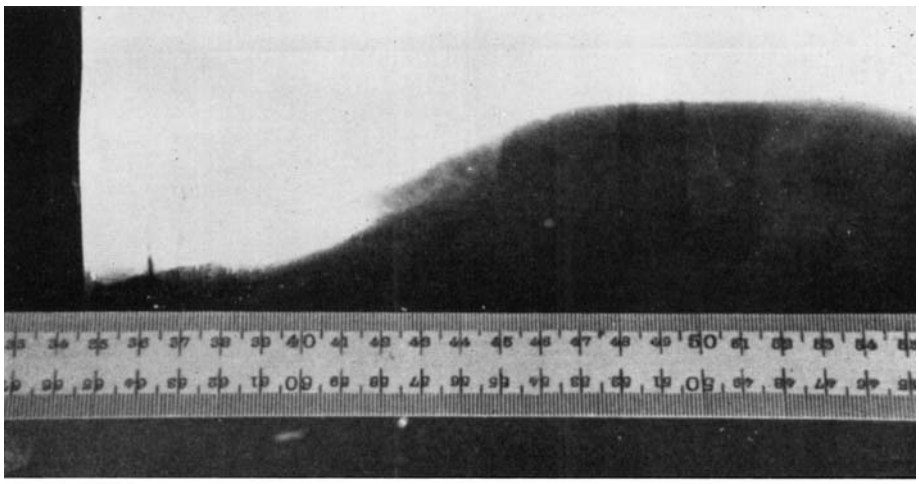

(*d*)

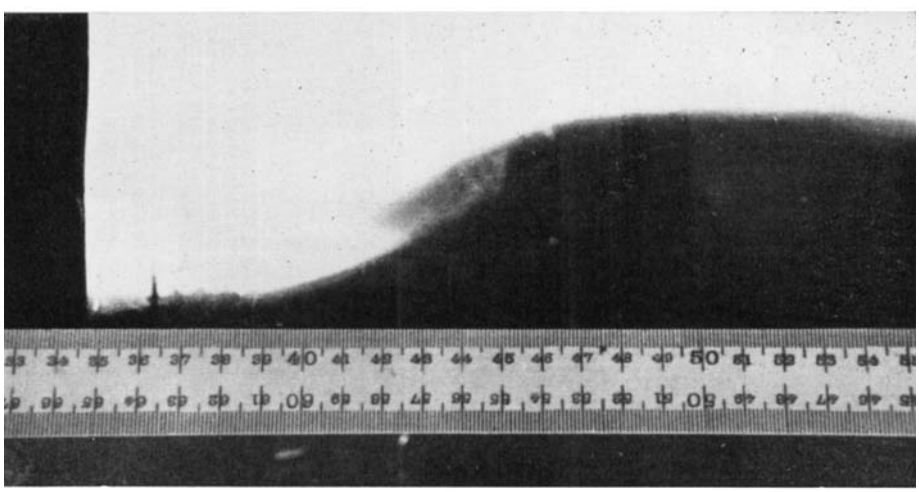

(*e*)

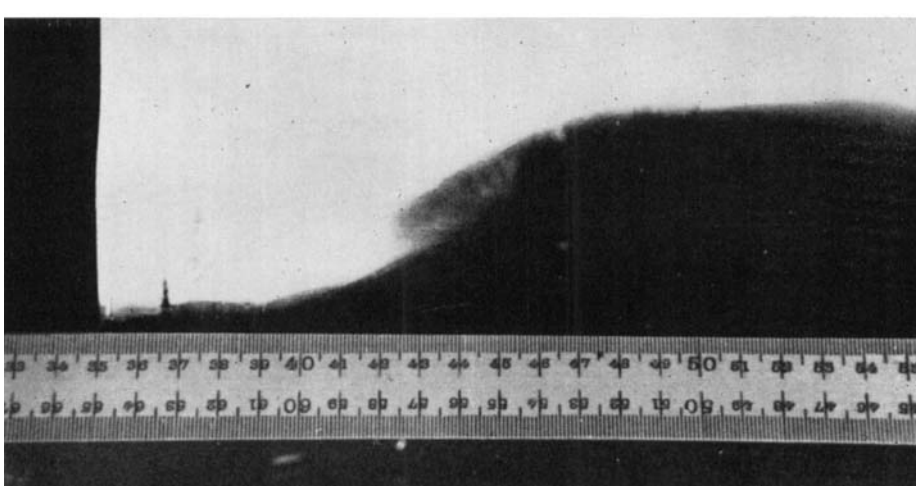

(*f*)

FIGURE 13. The development of instability at the interfacial wave node. Half the wave profile in mode $n = 2$ is shown. $h_1 = 25{\cdot}5$ cm, $h_2 = 19{\cdot}0$ cm, $\rho_2 - \rho_1 = 9{\cdot}0 \times 10^{-3}$ g/c.c. Total plunger amplitude = 0·9 cm. The photographs were taken at intervals of two or three oscillations.

THORPE

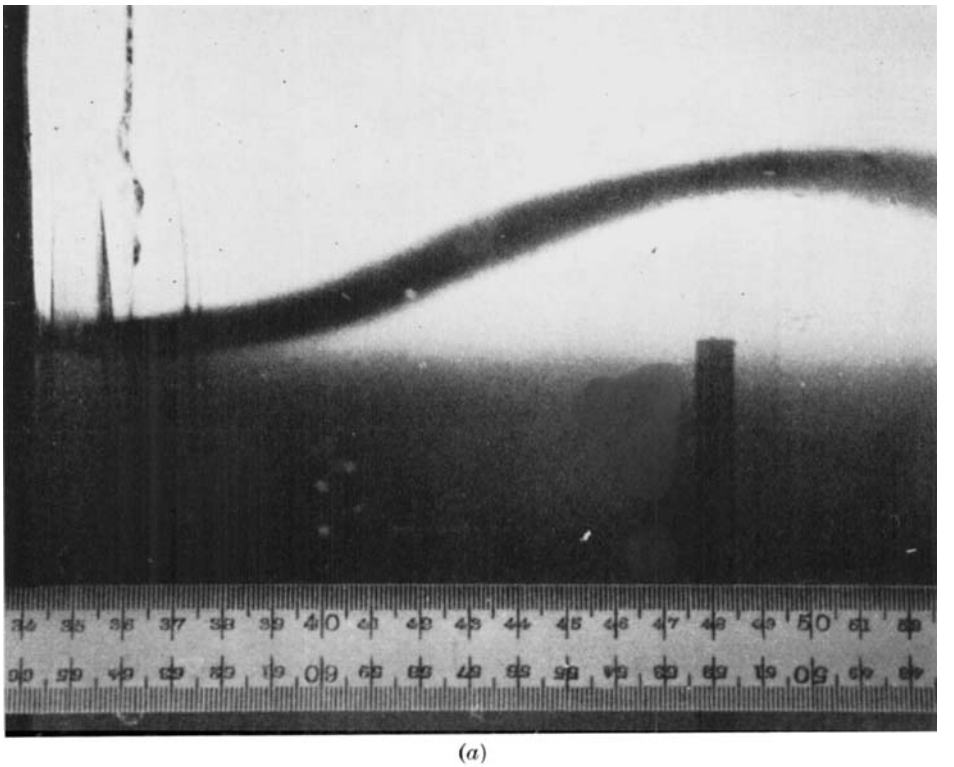

(*a*)

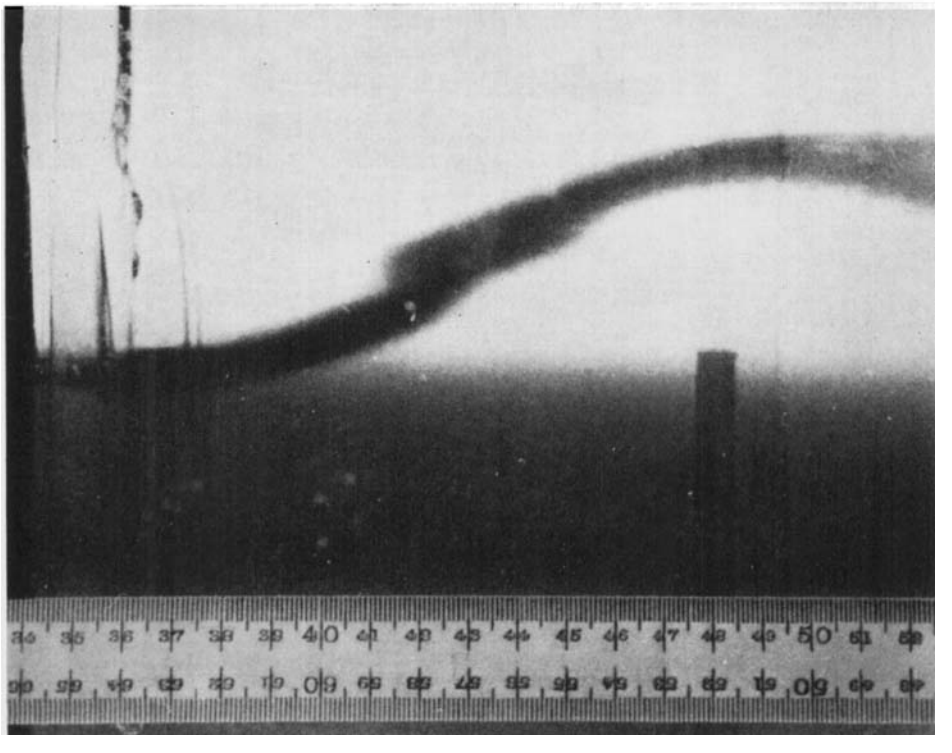

(*b*)

FIGURE 17. Layer of dye of intermediate density (*a*) before and (*b*) during the occurrence of irregularities at the wave node. Half the wave profile in mode $n = 2$ is shown.

THORPE

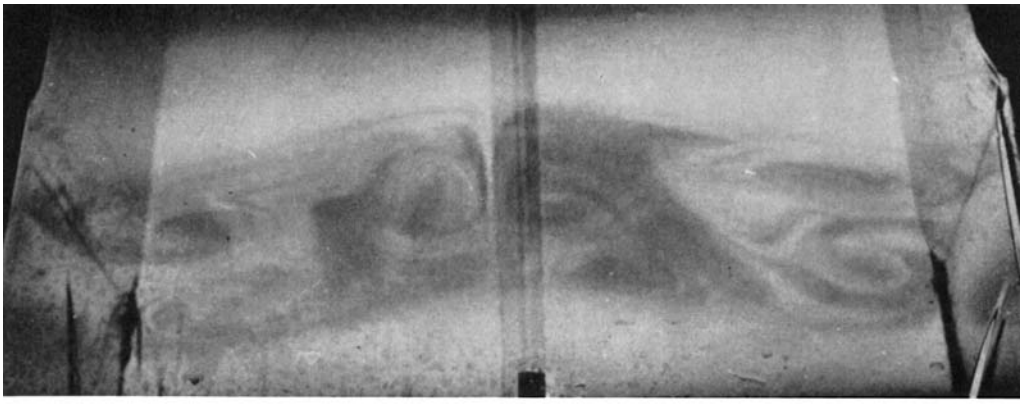

(*a*)

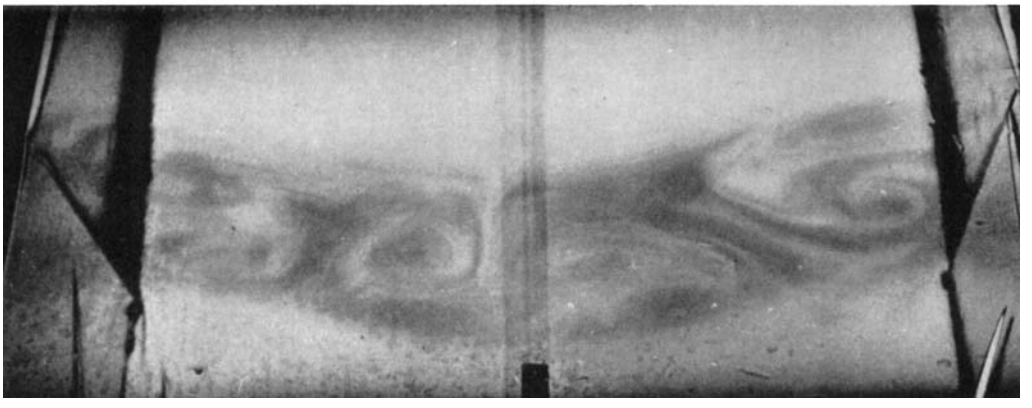

(*b*)

FIGURE 20. Streak patterns seen in a layer of coloured fluid at the interface between two fluids of different densities, looking upwards from below the level of the layer, when a standing wave of mode $n = 2$ is excited by the plunger motion. The side walls of the tank are seen in perspective. (*a*) 70th oscillation of the plungers, (*b*) 131st oscillation.

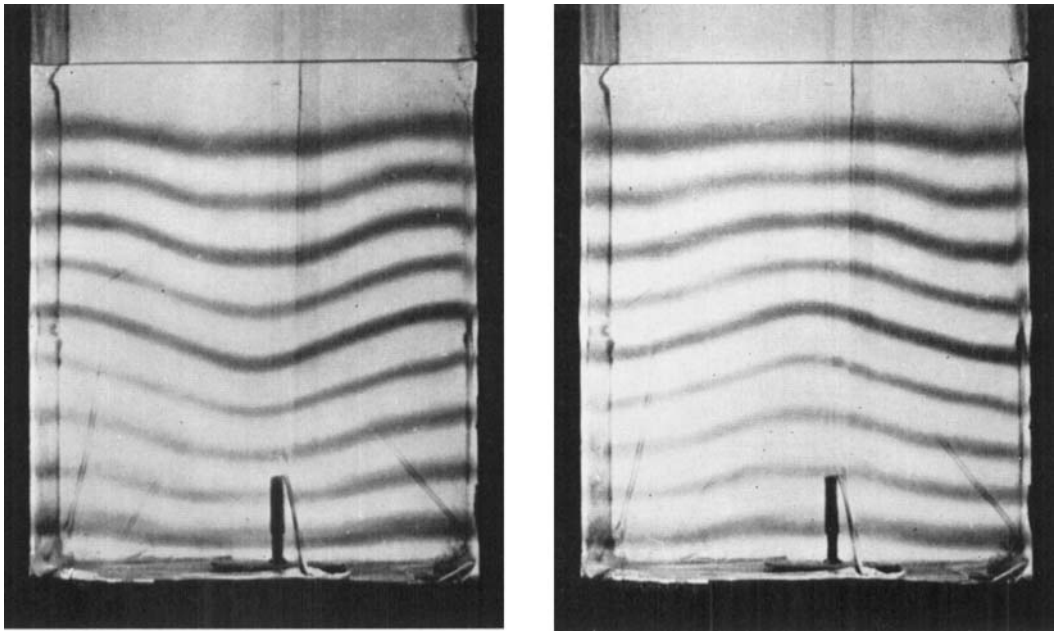

FIGURE 21. Standing waves at maximum displacements in a fluid of linear density gradient in free oscillation. The waves are made visible by the addition of gentian violet dye to the layers during the filling. Mode (2,1); $d\rho_0/dz = 5 \times 10^{-4}$ g/c.c./cm; $H = 40$ cm.

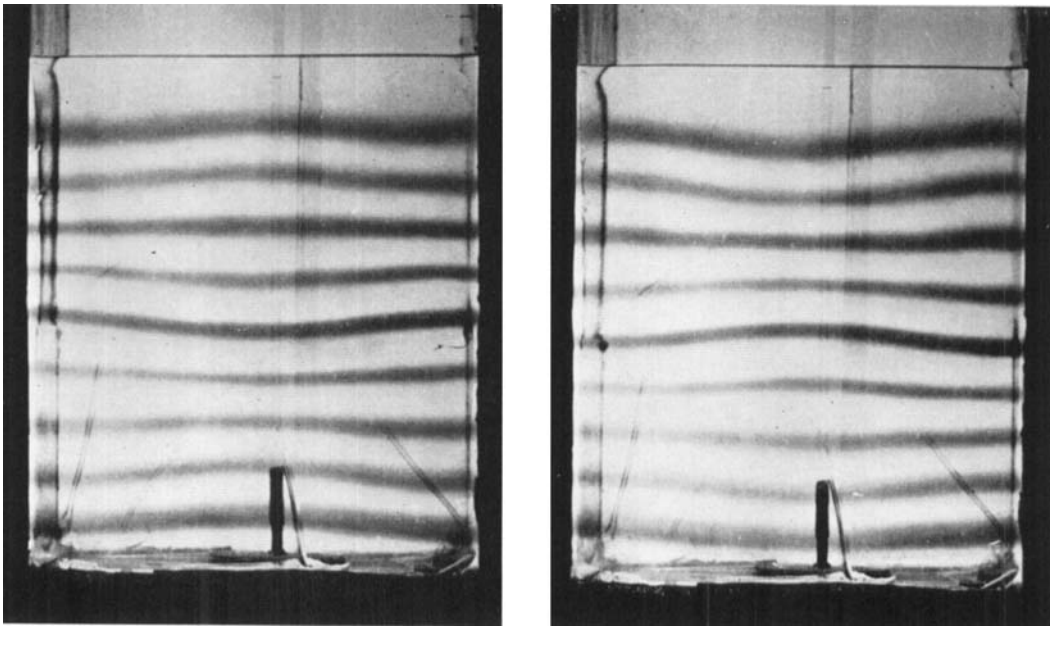

FIGURE 22. The mode (2,3) in free oscillation at times separated by half a wave period and at maximum displacement. Density gradient and depth as in 21.

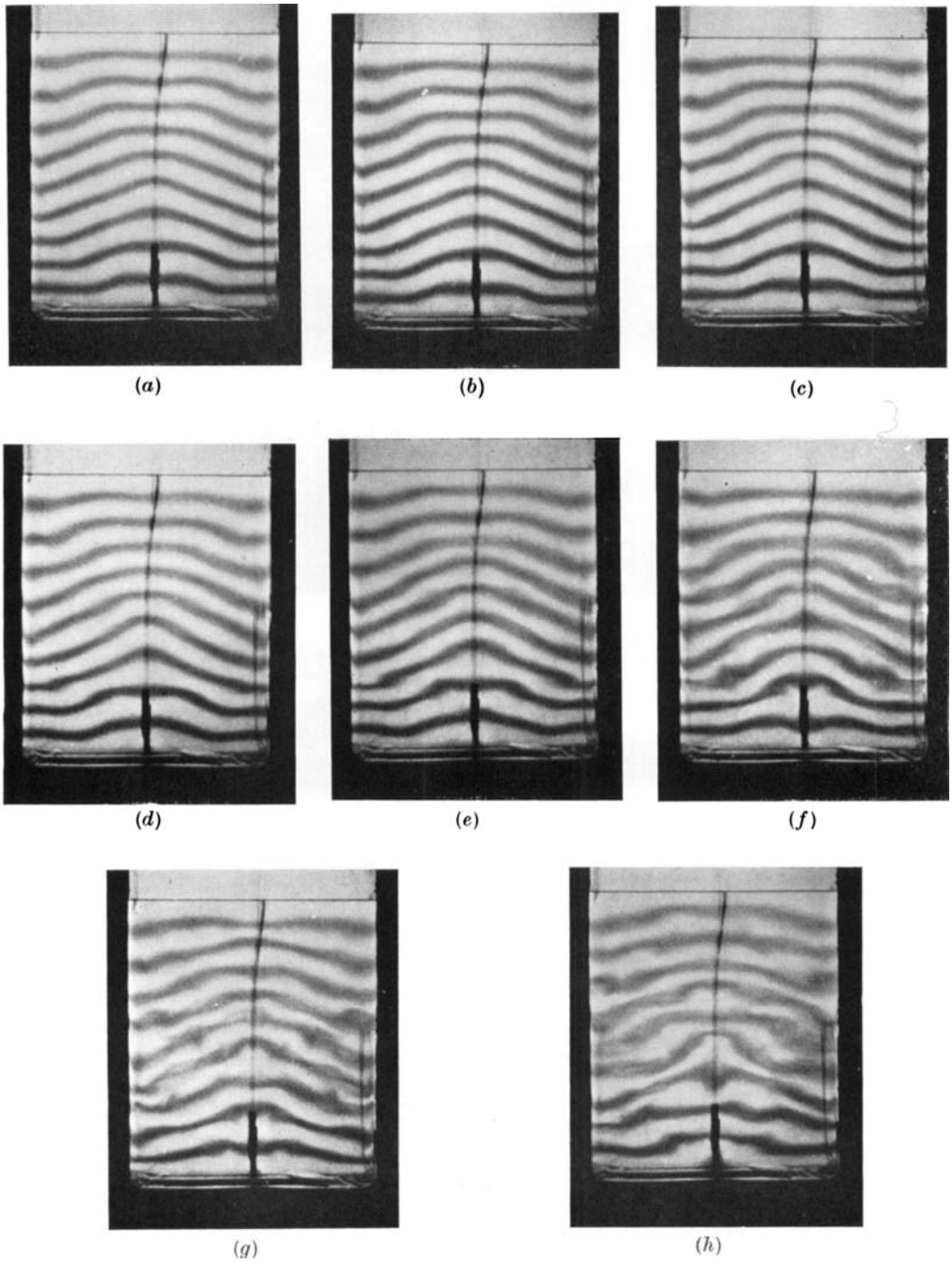

FIGURE 24. Sequence of photographs separated at time intervals of two oscillations showing the development of small scale irregularities in mode (2,1) with constant density gradient. Plungers moving in opposition with total amplitudes of 1·1 cm and frequencies of 0·628 rad/s.

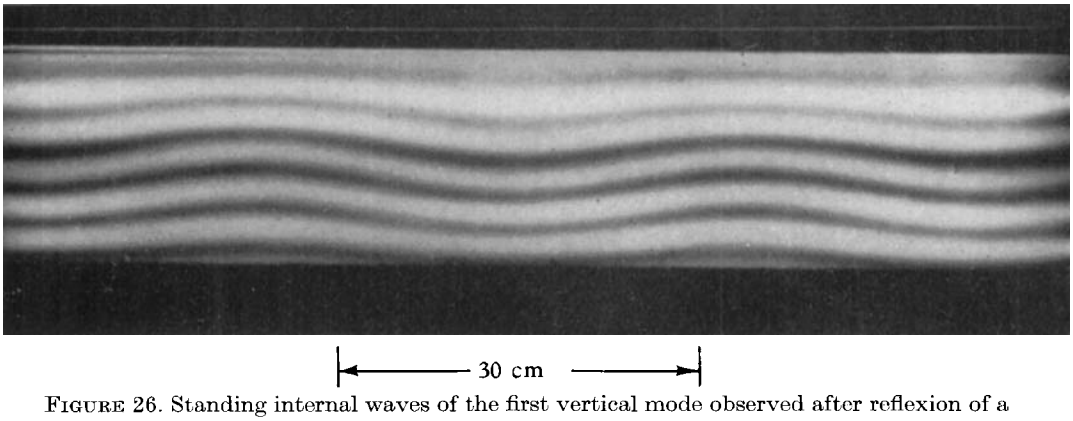

FIGURE 26. Standing internal waves of the first vertical mode observed after reflexion of a progressive wave at a vertical wall. The density gradient in the fluid is constant, $1{\cdot}00 \times 10^{-3}$ g/c.c./cm. The fluid depth is 21·5 cm and the wave frequency 0·711 rad/s.